Journal of Alloys and Compounds 657 (2016) 192–214

Contents lists available at ScienceDirect

Journal of Alloys and Compounds

journal homepage: http://www.elsevier.com/locate/jalcom

Calculated phase diagrams and thermodynamic properties of the Al_2O_3–Fe_2O_3–FeO system

Liya Dreval [a, b, c, *], Tilo Zienert [c], Olga Fabrichnaya [c]

[a] TU Bergakademie Freiberg, Institute of Energy Process Engineering and Chemical Engineering, Reiche Zeche Fuchsmühlenweg 9, 09599 Freiberg, Germany
[b] Metallurgical Department, Donbass State Engineering Academy, Shkadinova Street 72, 84313 Kramatorsk, Ukraine
[c] TU Bergakademie Freiberg, Institute of Material Science, Gustav-Zeuner Str. 5, 09599 Freiberg, Germany

ARTICLE INFO

Article history:
Received 14 June 2015
Received in revised form
15 September 2015
Accepted 2 October 2015
Available online 9 October 2015

Keywords:
Al_2O_3
Fe_2O_3
FeO
Spinel
Calphad-method

ABSTRACT

The thermodynamic description of the Al_2O_3–Fe_2O_3–FeO system has been developed considering newly available experimental data, as well as future compatibility of the present modeling with available descriptions of the Al–Fe, Al–O, and Fe–O systems. All of the experimental data available in the literature have been critically reviewed, and the inconsistent information has been excluded from the optimization. The sublattice model was applied to spinel phase to describe the degree of inversion in $FeAl_2O_4$–Fe_3O_4 solid solutions as well as an extension of homogeneity range in spinel by the dissolution of Al_2O_3 and Fe_2O_3. The thermodynamic parameters have been evaluated to describe the experimental data in the oxide part of the system.

1. Introduction

The Al_2O_3–Fe_2O_3–FeO system is of special industrial importance. The phase diagram of this system is widely applied to important metallurgical processes, such as deoxidation and ladle refining of molten steels [1,2]. The information on the phase relations is also important for understanding and analysis of thermite reactions between Al_2O_3 and iron [3], reactions of molten steel with refractories [4,5], and corrosion behavior of Al–Fe–Cr-based alloys [6]. The Al_2O_3–Fe_2O_3–FeO system is also of particular interest because of the presence of spinels, namely magnetite (Fe_3O_4), hercynite ($FeAl_2O_4$), and their solid solutions. Since minerals with spinel structure are widespread in nature, the crystal structure and thermodynamic properties of simple end-members such as magnetite and hercynite are especially important to geologists and mineralogists. A sound information on the aforementioned properties is crucial to a proper understanding of the behavior of more complex compositions (close to natural compositions). Magnetite and hercynite also occur in furnace smelting products, refractories, and in certain commercial sinters. Therefore, the modeling of interface reactions between steel melts and alumina-based filter materials is also important for the process of steel filtration [7]. It is essential to know the oxygen partial pressure at which spinel can appear as a stable phase during filtration.

The Al_2O_3–Fe_2O_3–FeO system is a complex object in particular for the thermodynamic modeling. On one hand, this system is not actually ternary since metallic iron exists as a phase at certain temperatures and compositions due to nonstoichiometry of wüstite. Thus, the corresponding equilibria must be taken into consideration to obtain reliable results. On another hand, iron reveals valences +2 and +3, and the Fe^{+2}/Fe^{+3} ratio is a function of temperature, composition, and partial pressure of oxygen p_{O_2}. In turn, the gas phase must be taken into account, and a complete representation of the system also requires accurate assessment of its potential diagrams. The thermodynamic assessments were carried out in Refs. [8,9]. Eriksson et al. [8] assessed the Al_2O_3–FeO phase diagram in equilibrium with iron, with all Fe^{+3} converted to "FeO". In their work, the spinel was considered as a solution of hercynite and metastable gamma alumina (γ–Al_2O_3) being described using the regular solution model. The modified quasichemical model was used for the liquid phase. In their work, the

* Corresponding author. TU Bergakademie Freiberg, Institute of Material Science, Gustav-Zeuner Str. 5, 09599 Freiberg, Germany.
E-mail addresses: liya.dreval@iww.tu-freiberg.de (L. Dreval), Tilo.Zienert@ww.tu-freiberg.de (T. Zienert), fabrich@ww.tu-freiberg.de (O. Fabrichnaya).

http://dx.doi.org/10.1016/j.jallcom.2015.10.017
0925-8388/

authors gave the probable maximum inaccuracy for the assessed diagram as ± 50 °C for the transformation temperatures, and ±2 at.% for the solid solubility. Decterov et al. [9] presented the calculations of multicomponent oxide systems within the computerized thermodynamic database for solid and liquid metal, slag, and solid oxide phases. Within the database, solid solutions were described by sublattice model in the framework of the Compound Energy Formalism (CEF), and the modified quasichemical model was applied to the liquid. Since the database comprises a vast number of systems, the discussion of applied models, and modeling results was very brief, particularly, for the Al_2O_3–Fe_2O_3–FeO system. The Al_2O_3–Fe_2O_3 phase diagram in equilibrium with air, Al_2O_3–FeO phase diagram in equilibrium with iron, and potential diagram at 1500 °C were presented along with experimental data. Thus, a thorough evaluation and modeling of the Al_2O_3–Fe_2O_3–FeO system is absent in the literature.

The aim of the present work is to perform a critical evaluation and thermodynamic assessment of the Al–Fe–O system. The present work is mainly focused on the oxide Al_2O_3–Fe_2O_3–FeO part of the system. The oxide part can be considered separately because the solid solutions and intermetallic phases of the Al–Fe system are stable only at very low oxygen partial pressure (10^{-42}–10^{-34} bar). Thus, the phase relations in metallic part and oxide part are separated from each other by the wide stability field of almost pure iron and Al_2O_3 [10]. However, due to the deviation from stoichiometry in wüstite phase metallic iron-based solid and liquid solutions with a small solubility of oxygen will be present in equilibria including wüstite. The thermodynamic models for solid iron dissolving oxygen will be included for the sake of the phase equilibria representation including non-stoichiometric wüstite. All solid phases except for $Al_2Fe_2O_6$ phase will be described using the compound energy formalism. Though, there are data on the homogeneity range of $Al_2Fe_2O_6$ phase it will be treated as stoichiometric compound due to the lack of crystallographic data about dependency of site occupancies on composition. The spinel phase will be treated as a continuous solid solution between magnetite and hercynite extending in the direction of Al_2O_3–Fe_2O_3 side of the composition triangle. The liquid phase will be described by partially ionic liquid that make it possible to describe metallic and oxide liquids as a single phase. The presented results are an important part of the project A03 of the Collaborative Research Centre SFB 920.

2. Selected data

The symbols to denote the phases are given in Table 1. For the cited experimental papers, the information on the methods and conditions is summarized in Tables 2 and 3. As the most of the experimental data were thoroughly reviewed in Ref. [11], a brief discussion of the results of principal experimental works is presented here.

2.1. Phases

FCC and BCC phases are iron-based solid solutions in the binary Fe–O system at a partial pressure of oxygen above 10^{-20} bar. As mentioned above, the solubility of Al is essential at substantially lower partial pressures of oxygen. At 1528 °C, solid iron (BCC) melts. Wüstite melts at lower temperatures (1370–1422 °C), and, therefore, at temperatures above 1528 °C metallic and oxide liquids are in equilibrium. In the binary system, the solubility of oxygen in solid and liquid iron is very small. In the ternary system, Trumble [12] evaluated the oxygen concentration in FCC phase at 951–1350 °C and in liquid metallic iron at 1550–1700 °C. The results show that the oxygen solubility in both phases is not high in the ternary system.

Wüstite is a non-stoichiometric phase in the binary Fe–O system. The maximal oxygen content in wüstite is 54.5 at.% [13]. Wüstite contains both divalent and trivalent iron ions, and the fraction of Fe^{+3} increases with the oxygen potential. The excess charge is compensated by vacancies in the phase. Wüstite decomposes to magnetite and BCC at the temperature of 556 °C [13]. In the ternary system, wüstite can dissolve some amount of Al_2O_3. At 1330 °C, the solubility of Al_2O_3 in the phase is 2 mol.% according to Fischer and Hoffman [14], and 1.3 mol.% according to Atlas and Sumida [15]. At 1000 °C, wüstite dissolves up to about 0.7 mol.% Al_2O_3. No dissolution of Al in wüstite was observed at 900 °C [16].

Corundum and hematite are stoichiometric compounds in the binary Al–O and Fe–O systems. Corundum is stable from its melting point until room temperature. Hematite decomposes to magnetite and oxygen at temperature 1452 °C in air [13]. The temperature of hematite decomposition depends on the partial pressure of oxygen. In the ternary system, the mutual solubility between Fe_2O_3 and Al_2O_3 is limited. The solubility of Fe_2O_3 in corundum and Al_2O_3 in hematite was measured by a number of authors [15,17–22] in the temperature range of 500–1550 °C in air. The agreement between different sources is satisfactory for the Fe_2O_3 solubility. However, the data of [15,20] show slightly lower Fe_2O_3 content in corundum compared to the results of [18,19,21]. As to the dissolution of Al_2O_3 in hematite, the experimental data exhibit some contradiction. According to the results of [15,17,19], the solubility of Al_2O_3 in hematite is much higher than it was established in Refs. [20,21]. Even at temperatures as low as

Table 1
List of the phases of the Al_2O_3–Fe_2O_3–FeO system.

Symbol	Phase description	Temperature range of phase stability in °C	Designation used in the thermodynamic database
L	Liquid		IONIC_LIQUID
BCC	Iron-based solution with b.c.c._A2 structure	<912; 1394–1538	BCC_A2
FCC	Iron-based solution with f.c.c._A1 structure	912–1394	FCC_A1
Wus	Wüstite, Fe (II) oxide, solid solution	556–1422	HALITE
Cor_F	Hematite, Fe (III) oxide, solid solution	<1452	CORUNDUM
Cor_A	Corundum, Al oxide, solid solution	<2054	CORUNDUM
$Spinel_m$	Magnetite, Fe (II, III) oxide, spinel structural group, and magnetite-based spinel solid solutions	<1597	SPINEL
$Spinel_h$	Hercynite, spinel structural group, and hercynite-based spinel solid solutions	<1780[a]	SPINEL
Spinel	Solid solution $Fe_{3-x}Al_xO_4$ at $x = 0$–2	<1774[a]	SPINEL
$Al_2Fe_2O_6$	$Al_2O_3 \cdot Fe_2O_3$ high-temperature compound	1317–1525[b]	FE2AL2O6

[a] The temperatures are calculated in the present work.
[b] The temperatures are calculated in the present work at $p_{O_2} = 1$ atm.

Table 2
Information on the methods and conditions of the phase relations experiments.

Reference	Experimental method	Experimental conditions
[14] [a]	Thermal analysis (TA), optical microscopy (OM), XRD	Mixtures of hematite and wüstite related to Al_2O_3–FeO section in equilibrium with iron. For mixtures with up to 10 wt.% Al_2O_3, iron crucibles are used. Al_2O_3 crucibles are used for compositions with 10–95 wt.% Al_2O_3.
[15] [a]	XRD, chemical analyses, optical pyrometry. Liquidus temperatures determined by direct observation of the liquid phase formation.	Iron boats were used for the samples containing iron phase or other metallic phase. Al_2O_3 crucibles were used for samples without metallic phases. He atmosphere. Samples with expected dissociation at low oxygen pressure were wrapped in Pt foil, sealed into fused-silica capsules under argon and heated in air. Samples along Al_2O_3–Fe_2O_3 section were heated in air or below 1370 °C (conditions that allow a small dissociation). T = 1000, 1220, 1240, 1250, 1275, 1325, 1350, 1366, 1370 °C Annealing time is 1–3 days.
[16]	Dynamic method	Mixtures Al_2O_3/Fe_2O_3 = 4/1, 2/1, 1/1, 1/3, T = 900 °C, CO/CO_2 atmosphere, Al_2O_3 boat.
[17]	X-ray diffraction method (XRD), Mössbauer spectroscopy	Mixtures of hematite and corundum, p_{O_2} = 0.21 atm., T = 1150 °C
[18]	Equilibration and quenching technique, OM, scanning electron microscopy with energy-dispersive spectra analysis (SEM-EDS), electron probe X-ray microanalysis (EPMA)	Mixtures of hematite and corundum related to Al_2O_3–Fe_2O_3 section, T = 1400, 1550 °C, p_{O_2} = 0.21 atm.
[19]	Equilibration and quenching technique, OM, SEM-EDS, EPMA	Mixtures of hematite and corundum related to Al_2O_3–Fe_2O_3 section, T = 1200, 1300, 1400 °C, p_{O_2} = 0.21 atm.
[20]	Oxygen loss determination by direct weighing OM, XRD	T = 1200–1500 °C, p_{O_2} = 0.21 atm. 1380, 1390, 1400, 1430, 1440, 1460 °C, p_{O_2} = 0.21 atm.
[21]	Quenching technique, XRD, OM, optical pyrometry. Liquidus temperatures determined of the strip furnace by direct observation of the complete flow of the sample. Solidus temperatures determined by observing the sintering temperature of the sample kept just below the solidus to permit equilibrium ratio of Fe^{+2}/Fe^{+3}. Total iron content is determined by the Zimmermann-Reinhardt method, divalent iron is determined by the divalent gravimetric method	Mixtures of hematite and corundum related to Al_2O_3–Fe_2O_3 section at p_{O_2} = 0.21, 1 atm. Platinum envelopes or platinum crucible preliminary saturated with iron were used.
[22]	Experimental technique of buffering hydrogen and oxygen fugacities within hydrothermal pressure vessels, XRD, OM	T = 500–900 °C, total pressure is 1, 2, 4 kb. Equilibration time 1–94 days
[23]	Rietveld refinement of XRD data	Synthetic hercynite with a small amount of Fe_2O_3 equilibrated at T = 850 °C
[24]	XRD	Synthetic hercynite with a small amount of Fe_2O_3 annealed at T = 900 °C
[25]	In-situ time-of-flight neutron powder diffraction, Rietveld refinement	Hercynite, T = 25–1150 °C, vacuum
[26]	Rietveld refinement of XRD data, Mössbauer spectroscopy, neutron diffraction measurements	Synthetic hercynite with a small amount of Fe^{+3}, T = 500–1200 °C, equilibrated with CO/CO_2 mixtures. At 500 and 550 °C, samples were cooled down in the air. At higher temperatures, samples were quenched into the water.
[27] [a]	XRD, petrographic method, OM, optical constants of corundum measurements. Liquidus temperatures are determined using the pyrometric cones to follow the softening process.	Mixtures of hercynite and corundum related to Al_2O_3–FeO section, Ar atmosphere, Al_2O_3 and ZrO_2 tubes. For OM, XRD investigations, sintering temperature is 1200, 1700 °C, sintering time is 6–10 h.
[28]	Thermogravimetric, XRD	$p_{O_2} = 1.8 \cdot 10^{-3}$ atm. at 1300, 1400, 1500 °C (CO_2 atmosphere), $p_{O_2} = 4.0 \cdot 10^{-7}$, $7 \cdot 10^{-10}$ atm. at 1500 °C (CO/CO_2 atmosphere)
[29]	XRD	T = 1280, 1380, 1500 °C, CO/CO_2 or Ar/O_2 atmosphere, five dense spinel of various cation compositions
[32]	Combination of thermopower and electrical conductivity measurements	Samples $(Fe^{+2})(Fe^{+3})_{2x}Al_{2-2x}O_4$ with x = 0.25, 0.5, 0.75, 1.00, T = 600–1400 °C, (CO/CO_2 atmosphere)
[33]	Mössbauer spectroscopy	Samples $Fe_{3-x}Al_xO_4$ with x = 0, 0.05, 0.1, 0.3, 0.6, 0.9, cooled with furnace from 1350 °C, $p_{O_2} = 7 \cdot 10^{-4}$ atm.
[34]	Seebeck coefficient measurements	Samples $Fe_{3-x}Al_xO_4$ with x = 0.49, 0.97, 1.46, T = 1327 °C
[36]	Quenching technique, XRD, OM	T = 1335, 1341, 1402, 1409 °C, p_{O_2} = 0.063, 0.4 atm., CO_2 atmosphere. Annealing time is 1–3 days
[37] [a]	Equilibration of Al_2O_3–FeO slags in the corundum crucible with solid or liquid iron, TA	Mixtures related to Al_2O_3–FeO section in equilibrium with iron
[38] [a]	Quenching technique	Mixtures of hematite and wüstite related to Al_2O_3–FeO section, Ar atmosphere
[39] [b]	Quenching technique, SEM, XRD	Mixtures of hematite and wüstite related to Al_2O_3–FeO section, Ar atmosphere, Al_2O_3 tube, molybdenum foils.
[42]	Equilibration experiments between liquid iron, hercynite, and alumina crucible	T = 1575–1750 °C, He atmosphere

[a] Fe^{+3} was not recalculated to FeO.
[b] Fe^{+3} was recalculated to FeO.

Table 3
Information on the experimental investigations of thermodynamic properties.

Reference	Experimental method	Studied thermodynamic properties	Experimental conditions
[30]	Emf measurements, galvanic cell with solid electrolyte	Activity of Fe_3O_4 and $FeAl_2O_4$	T = 700, 870, 900, 1000 °C
[31]	Gas-metal-oxide equilibration technique	Activity of Fe_3O_4 and $FeAl_2O_4$, p_{O_2}	T = 1300 °C, CO/CO_2 streams, Pt foils, mixtures of magnetite and hercynite
[43]	Emf measurements, solid oxide galvanic cells with $CaO–ZrO_2$ and $CaO–ZrO_2$ in combination with $YO_{1.5}–ThO_2$	p_{O_2}	T = 750–1390 °C, hercynite + Fe_s + corundum, Al_2FeO_4 + Fe_L assemblages, Ar gas flow[a]
[44]	High-temperature oxide-melt solution calorimetry	Enthalpy of formation for $Al_2Fe_2O_6$, mixing enthalpies of solid solutions	T = 25, 702 °C, $Al_2Fe_2O_6$ compound, hematite, corundum
	Differential scanning calorimetry	Heat capacity	T = 25–1277 °C, $Al_2Fe_2O_6$ compound
[45] [b]	Gas-metal-oxide equilibration technique, chemical analysis	Activity of FeO	T = 1400 °C, iron crucible, H_2/H_2O mixtures
[46] [c]	Gas equilibration technique, SEM-EDS analysis, atomic absorption spectroscopy, X-ray fluorescence spectroscopy, Mössbauer spectroscopy	Activity of FeO	T = 1550, 1600 °C, CO/CO_2/Ar mixtures, platinum crucible
[47]	Heat capacity calorimeter	Heat capacity	T = (−222)–25 °C, hercynite
[48]	Low-temperature calorimetry	Heat capacity	T = (−269)–127 °C, synthetic polycrystalline hercynite with a small amount of Fe^{+3}

[a] Fe_s and Fe_L is the designation for solid and liquid iron.
[b] Fe^{+3} was recalculated to FeO.
[c] Fe^{+3} was not recalculated to FeO.

500–800 °C, Turnock and Eugster [22] measured solubility of Al_2O_3 in hematite as high as ~5–10.5 mol.% Al_2O_3.

In the ternary system, spinel is a solid solution of magnetite (Fe_3O_4), hercynite ($FeAl_2O_4$), Fe_2O_3 and Al_2O_3. Spinel has tetrahedral (T) and octahedral (O) sites in which Al^{+3}, Fe^{+2}, Fe^{+3} are distributed indicating the different degree of inversion (content of trivalent cation in tetrahedral site). Therefore, spinel can be described by the following model $(Al^{+3}, Fe^{+2}, Fe^{+3})^{T}_{1}(Al^{+3}, Fe^{+2}, Fe^{+3}, Va)^{O}_{2}O_4$, where Va is vacancies introduced to describe the deviation of oxygen content towards Al_2O_3 and Fe_2O_3. It is important to note that magnetite and hercynite have different degree of inversion.

Magnetite is an inverse spinel with the tetrahedral sites filled by Fe^{+3}, and the octahedral sites by both Fe^{+3} and Fe^{+2} in ratio 1/1. With increasing temperature, the degree of inversion in magnetite (amount of Fe^{+3} in tetrahedral sites) gradually changes from value close to 1 (inverse spinel) to value of 0.667 which corresponds to random distribution of Fe^{+2} and Fe^{+3} between tetrahedral and octahedral sublattices. Magnetite has a deviation from its ideal stoichiometry towards higher and lower oxygen content in the range from 57.1 at.% O at 1422 °C up to 58 at.% O at 1452 °C [13].

Hercynite is a spinel phase close to normal spinel with Fe^{+2} predominantly on the tetrahedral sites and with Al^{+3} predominantly on the octahedral sites at room temperature. The cation distribution in hercynite with temperature was measured by a number of authors [23–26]. The experimental results [23–26] show that the amount of Al^{+3} in a tetrahedral site (degree of inversion) is increasing with temperature. For hercynite, there are several important factors influencing the results of such investigations that must be discussed. First of all, the effect of the occurrence of Fe^{+3} in hercynite on the cation distribution in this substance can be very large. This must be considered in the case of results [23,24,26] who reported the presence of Fe^{+3} in their samples (up to 3% from Mössbauer measurements [26]). Another point is that the obtained experimental results do not actually correspond to equilibrium cation distribution at low temperatures because of the low atomic mobility. For example, Harrison et al. [25] discussed that equilibrium values were not achieved for the temperatures up to 600 °C. The last point to mention is an anomalously fast rate of re-ordering at high temperatures which occurs during rapid cooling. This results in a substantial degree of cation redistribution during quenching. As a result, an as-quenched cation distribution differs from equilibrium cation distribution at the annealing temperature [26]. For these reasons, results of [25] who used in-situ measurements can be regarded as the most reliable. Hercynite is unstable at low partial pressures of oxygen and decomposes into solid iron and corundum. According to [14,27,28], hercynite can dissolve the excess amount of Al_2O_3. The solubility is 5.8 mol.% Al_2O_3 at 1750 °C, and equal to zero at 1500 °C [14]. The observation of [14] were supported by results of [27] who show that at least 5.4 mol.% Al_2O_3 can be dissolved in hercynite at 1750 °C. Roiter [28] show that this phase dissolves up to 3 mol.% Al_2O_3 at 1500 °C, which is much higher in Al_2O_3 content in comparison with data [14,29].

In the ternary system, a continuous solid solution exists between magnetite and hercynite in a wide temperature range [15,20,28–31]. In the temperature range 1000–1500 °C, this spinel solid solution deviates considerably from its stoichiometry $FeAl_2O_4–Fe_3O_4$ towards excess oxygen content due to dissolution of Al_2O_3 and Fe_2O_3 [15,20,21,28]. Below 1000 °C, there are no relevant data as to the excess oxygen solubility. The distribution of cations between tetrahedral and octahedral sites in solid solution has been determined by Nell et al. [32] at 600–1400 °C. Dehe et al. [33] presented experimental data on the amount of Al^{+3} on tetrahedral sites at 1350 °C. From the data on Seebeck coefficient, Mason [34] also estimated fractions of different species on tetrahedral and octahedral sublattices in spinel solid solution at 1327 °C. According to their experimental results on tetrahedral sublattice, the amount of Fe^{+2} cations is increasing while the amount of Fe^{+3} cations is decreasing with the composition changing from magnetite to hercynite. For octahedral sublattice, the amount of both Fe^{+2} and Fe^{+3} cations is decreasing while the composition is approaching hercynite. These observations are in good agreement with the fact that magnetite is an inverse spinel, and hercynite is a normal spinel. It must be noted that the cation distribution obtained by Dehe et al. [33] can differ from equilibrium one at the annealing temperature since the samples were cooled down with the furnace. Spinel continuous solid solution decomposes into magnetite-rich and hercynite-rich spinels. Turnock and Eugster [22] gave the

coordinates of the critical point of spinel solid solution decomposition as 860 ± 15 °C at 28 mol.% Al_2O_3, 22 mol.% Fe_2O_3 and 50 mol.% FeO. The solvus was determined in the temperature range of 500–850 °C [22]. However, the authors pointed out that equilibrium was not approached at 500 °C.

An $Al_2Fe_2O_6$ compound related to the ternary system has an orthorhombic crystal structure [15,35] and undergoes a structural transformation at temperatures ~1320–1335 °C [15]. According to Muan and Gee [21], the upper-temperature limit of the stable existence of compound is 1410 °C in air and of 1490 °C at 1 atm. O_2. There is a disagreement between different literature data as to the low-temperature stability of $Al_2Fe_2O_6$. In air, the temperature of 1318 and 1320 °C were given by Muan and Gee [21], and Atlas and Sumida [15], respectively. On the other hand, the recent data of Rhamdhani et al. [19] show that this phase is stable at a temperature of 1300 °C in air. $Al_2Fe_2O_6$ compound has a homogeneity range. According to [21], this region extends from ~47 mol.% Al_2O_3 at 1410 °C up to ~54 mol.% Al_2O_3 at 1380 °C in air. At 1370 °C, Atlas and Sumida [15] gave values from 40 up to 53 mol. % Al_2O_3 that are higher in Fe_2O_3 content in comparison with [21]. The results of [18,19] show that the solubility of Al_2O_3 in the phase is higher than that established in Ref. [21]. The observed upper limit of Al_2O_3 dissolution in $Al_2Fe_2O_6$ phase was given as 53 mol. % [18] and 56.5 mol. % [19] at 1400 °C in air. From data of Muan and Gee [21] at 1 atm. O_2, the homogeneity range of $Al_2Fe_2O_6$ compound varies from ~47 mol.% Al_2O_3 at ~1490 °C up to ~55 mol.% Al_2O_3 at 1440 °C.

2.2. Vertical sections

2.2.1. Al_2O_3–Fe_2O_3 section in air and pure oxygen atmosphere

The phase equilibria data for the Al_2O_3–Fe_2O_3 system were obtained in Refs. [18–21,36]. The investigations of Muan and Lee [21] were performed in air and pure oxygen atmosphere. The experimental data of Muan [36] were established by quenching method at a partial pressure of oxygen 0.4 and 0.063 atm. All other authors conducted their researches in air. This experimental information does not correspond to the real binary Al_2O_3–Fe_2O_3 system, as there will be a significant amount of Fe^{+2} present in the liquid phase and the presence of the spinel phase that belongs to the center of the Al_2O_3–FeO–Fe_2O_3 system. However, the section at a constant partial pressure of oxygen resembles the true binary diagram in the temperature range where spinel phase is no longer stable. For these reasons, the results at a constant partial oxygen pressure were presented as the diagram resembling binary one in Refs. [18,19,21]. The details as to the construction of these diagrams can be found in Ref. [21]. The main results of these works could be summarized as follows.

In the earlier work of Richards and White [20], the existence of $Al_2Fe_2O_6$ was not reported for the temperatures 1300–1400 °C. In this temperature range, the authors interpreted their results as equilibria between spinel, hematite, and corundum that is in a disagreement with all later data of [15,18,19,21]. According to these works, the high-temperature limit of $Al_2Fe_2O_6$ stability corresponds to its decomposition into spinel and corundum. This temperature increases from 1410 to 1490 °C with increasing of p_{O_2} from 0.21 to 1 atm [21]. The low-temperature limit of the phase stability corresponds to $Al_2Fe_2O_6$ decomposition into hematite and corundum (1315 °C at $p_{O_2} = 0.03$ atm. [36], and 1318 °C at $p_{O_2} = 0.21$ and 1 atm. [21]). The data of [21,36] at different partial pressures of oxygen implies that the temperature of $Al_2Fe_2O_6$ decomposition into corundum and hematite is slightly dependent on a partial pressure of oxygen.

According to the data of [18–21,36], the mutual solubility of Al_2O_3 and Fe_2O_3 is increasing with temperature. Considering results of Muan and Gee [21] at different partial pressures of oxygen, one can conclude that the limits of mutual solubility of Al_2O_3 and Fe_2O_3 are not dependent on the p_{O_2} values. Along the Al_2O_3–Fe_2O_3 section in air and pure oxygen atmosphere, the temperature of hematite decomposition is decreasing with the increase of Al_2O_3 concentration [21]. The lowest temperature corresponds to the decomposition of spinel into hematite and $Al_2Fe_2O_6$ and depends on the partial pressure of oxygen (1380 °C in air, 1440 °C at 1 atm. O_2 [21]).

Along the Al_2O_3–Fe_2O_3 section in air, the position of the phase lines for the spinel field was determined in Refs. [19–21]. The results are in good agreement with each other. The solubility of Al_2O_3 in spinel is increasing with the temperature increase.

2.2.2. Al_2O_3–FeO section in equilibrium with iron

Due to the deviation of wüstite composition from the ideal stoichiometry, samples with an average composition corresponding to the Al_2O_3–FeO system contain some amount of liquid or solid metallic iron. However, experimental results are often represented in a way resembling a quasi-binary diagram.

The Al_2O_3–FeO section was investigated by a number of authors [14,15,27,37–39]. The presence of solid iron in the samples was confirmed by the results of Oelsen and Heynert [37], Fischer and Hoffman [14], and Rosenbach and Schmitz [39]. The later recalculated all amount of iron to FeO. As a result, their liquidus temperatures were shifted towards higher FeO content in comparison with those obtained in Refs. [14,15,27,37,38]. Atlas and Sumida [15], Novokhatsky et al. [27], and Galakhov [38] took a special precaution of keeping the amount of Fe^{+3} cations as low as possible. All the authors represented phase equilibria as a quasi-binary Al_2O_3–FeO system.

Two alternative variants of hercynite formation from liquid phase were suggested by the authors. Oelsen and Heynert [37] concluded that a peritectic formation takes place for hercynite at 1750 °C from their thermal analysis measurements. On the contrary, congruent melting was proposed by Fischer and Hoffman [14] at 1780 °C, by Novokhatsky et al. [27] at 1820 ± 15 °C, by Galakhov [38] at 1800 °C, and by Rosenbach and Schmitz [39] 1765 ± 15 °C. Consequently, the invariant equilibrium of eutectic type liquid ↔ hercynite + Al_2O_3 was established by Fischer and Hoffman [14] at 1750 °C (with 57 mol.% Al_2O_3 in liquid phase), by Novokhatsky et al. [27] 1750 ± 15 °C, and by Galakhov [38] at 1750 °C (with 56 mol.% Al_2O_3 in liquid phase). Rosenbach and Schmitz [39] also represented this phase diagram as of eutectic type. For the liquidus temperatures determined by the different authors [14,27,37–39], the agreement is satisfactory.

The occurrence of the eutectic reaction liquid ↔ wüstite + spinel was established by Fischer and Hoffman [14] at 1330 °C (with 3.6 mol.% Al_2O_3 in liquid phase), by Novokhatsky et al. [27] at 1310 ± 10 °C, and by Oelsen and Heynert [37] at 1325 °C.

Fischer and Hoffman [14] and Novokhatsky et al. [27] also provided data about FeO dissolution in corundum. According to Fischer and Hoffman [14], the solubility of FeO in corundum is 9 mol.% at 1750 °C, and 2 mol.% at 1500 °C. From their measurements of optical constants of Al_2O_3, Novokhatsky et al. [27] concluded that the solubility of FeO in corundum lays outside the limits of the sensitivity of the method (3 at.%) even at temperatures as high as 1750 °C.

2.3. Isothermal sections

The phase equilibria in the Al_2O_3–Fe_2O_3–FeO were studied in Refs. [15,20,28] in the temperature range 1000–1500 °C and in Ref. [22] at 500–900 °C. The formation of the continuous solid solution of spinel extending in the direction of Al_2O_3–Fe_2O_3 side was confirmed in Refs. [15,20,28]. The extension of the spinel solid solution towards the Al_2O_3–Fe_2O_3 side is decreasing with

temperature [15,20,28]. According to Atlas and Sumida [15], spinel solution is in equilibrium with a liquid phase and solid iron at 1350 °C. The three-phase equilibria spinel + cor_A + cor_F, spinel + wüs + Fe_s appear at 1000 and 1250 °C [15]. In the temperature range below the temperature of spinel solid solution decomposition (860 °C), magnetite-based spinel is in equilibrium with corundum and hematite while hercynite-based solid solution is in equilibrium with wüstite and solid iron [22].

2.4. Potential diagram

The potential diagrams were proposed in Refs. [22,29,31,40]. It should be noted that Meyers et al. [29] also used the data from Refs. [14,15,21,28,36,40] for the construction of the diagrams at 1280, 1380, and 1500 °C. The obtained results are in good agreement except for the data of [28] which are higher in Al_2O_3 concentration in comparison with data of [29]. The reasons can be that the boundary position in Ref. [28] was determined indirectly by graphically extrapolation of the thermogravimetric results.

The authors [22,29,31,40] focused on the investigation of the stability ranges of the spinel solid solution as a function of p_{O_2}. From these experimental data, it is evident that the continuous solid solution exists in the range of partial pressures of oxygen. The lowest value of p_{O_2} corresponds to the equilibrium between hercynite, corundum, and solid iron. A number of authors [20,22,28,41–43] presented the values of p_{O_2} for this equilibrium. According to these data, the equilibrium partial pressure of hercynite decomposition is increasing with temperature. At high partial pressures of oxygen, spinel is in equilibrium with hematite and corundum, or hematite and $Al_2Fe_2O_6$, or corundum and $Al_2Fe_2O_6$. Turnock and Eugster [22] also presented the values of equilibrium oxygen pressure for the invariant equilibria including magnetite-based and hercynite-based spinels at temperatures below 900 °C.

2.5. Thermodynamics

Majzlan et al. [44] measured the mixing enthalpies of the hematite-corundum solid solution at 25 °C and 702 °C. The positive values of this function correlate well with the existence of immiscibility gap between Fe_2O_3 and Al_2O_3 components. From the data for different temperatures, the authors concluded that the mixing enthalpy is independent of temperature.

The thermodynamic properties of $Al_2Fe_2O_6$ compound were investigated by Majzlan et al. [44]. The enthalpy of formation of this compound from oxides was determined at 25 °C by high-temperature oxide melt solution calorimetry. The reported value is 55800 J mol^{-1}. Using differential scanning calorimetry, the heat capacity of the compound was also measured for the temperature range 25–1277 °C. The value of the standard entropy of 197.6 J mol^{-1} K^{-1} was also estimated as the sum of the assessed vibrational entropy (75.2 J mol^{-1} K^{-1}), magnetic entropy (14.9 J mol^{-1} K^{-1}), dilatation entropy (0.38 J mol^{-1} K^{-1}), and configurational entropy (8.42 J mol^{-1} K^{-1}). From their thermodynamic data, authors deduced that $Al_2Fe_2O_6$ compound is unstable at 25 °C with respect to hematite and corundum.

The activities of FeO in slags were measured in Ref. [45] at 1400 °C and, recently, in Ref. [46] at 1550, 1600 °C using gas equilibration technique. A negative deviation from Raoult's law was observed at corundum content higher than 3.6 mol. %. From their experimental results on the phase equilibria in the system, Schmahl and Dillenburg [16] estimated activities of the components in the spinel solid solution at 900 °C. The activities data for magnetite are available from the measurements of [31] at 1300 °C, and later one of [30] at 900, 1000 °C. Lykasov and Kimyaschev [30] also gave evaluated activities of magnetite and hercynite at 700 and 800 °C. From the data of [30,31], it is evident that the deviations from ideality for the activities of components in spinel solid solution gradually changes from slightly negative at 1300 °C to strongly positive at below 1000 °C. This tendency is in agreement with the presence of spinel solid solution in the high-temperature region of the phase diagram and spinel decomposition below 860 °C. The negative deviations of the activities of Fe_3O_4 and $FeAl_2O_4$ proposed in Ref. [16] at 900 °C could be questionable since these findings contradict the existence of the spinel miscibility gap at this temperature.

The low-temperature heat capacity of hercynite was measured in Refs. [47] and [48] at (−270)–(127) °C. The standard entropy of formation was also established in both works. For the low-temperature heat capacity, the agreement between the experimental values is excellent. The calculated value of the standard entropy of [48] (113.9 ± 02 J mol^{-1} K^{-1}) is higher than that of [47] (106.3 J mol^{-1} K^{-1}). The standard entropy of hercynite was also estimated in Ref. [43] as 108 ± 1 J mol^{-1} K^{-1}. The assessed values of the standard entropy of hercynite and enthalpy of formation of hercynite from elements in geological databases were based on phase equilibria between minerals. They varied from 106 to 123 J mol^{-1} K^{-1} for S°_{298} and from −1945000 to −1966000 J mol^{-1} for $\Delta_f H_{298}$ [49–55]. The enthalpy of formation of hercynite was also evaluated in Ref. [43] from the reaction Fe_s + $1/2O_2$ + Al_2O_3 = hercynite in the temperature range of 750–1536 °C. Assuming that ΔC_p of this reaction is equal to zero, and taking into account the enthalpy of formation of corundum, the value obtained in Ref. [43] using EMF measurements was recalculated into the enthalpy of formation of hercynite from pure elements as −1968000 J mol^{-1} in the present work to compare with other available data. The experimental data on the high-temperature heat capacity of hercynite was not reported so far. However, the assessed values of C_p for hercynite can be found in different databases for minerals, for example, in Ref. [55].

In current assessment, the data of [14,15,17–19,21–27,29,37–40,42] on the phase equilibria and results of [30,31,43–48] on the thermodynamic properties of the phases were used. Since we did not aim to describe the homogeneity range of $Al_2Fe_2O_6$ compound in the present work, the relevant data of [15,18,19,21] were not considered. The data of [20] obtained in the temperature range 1300–1400 °C were discarded because of their contradiction to the results of [15,18,19,21]. The data of [16] on the thermodynamic activities and the data of [28] on the phase equilibria were excluded from optimization because of a disagreement with the other relevant data [30,31] and [14,29]. All the data accepted in the present work were further analyzed during the thermodynamic description of the system.

3. Thermodynamic models

3.1. Solid solutions

The thermodynamic models and parameters for wüstite, hematite, corundum phases were compiled from Refs. [13,56]. For BCC and FCC phases, the model and parameters were accepted according to [13].

All solid solutions are described using the compound energy formalism. For wüstite, the two-sublattice model was used. The species Al^{+3}, Fe^{+3}, Fe^{+2} are mixed on the first sublattice; oxygen completely occupies the second sublattice. In the first sublattice, the vacancies are also considered to accommodate the species Al^{+3} and Fe^{+3} in this sublattice and keep the electroneutrality. The final model for wüstite is $(Al^{+3}, Fe^{+3}, Fe^{+2}, Va)_1(O^{-2})_1$. The two-sublattices $(Al^{+3}, Fe^{+3})_2(O^{-2})_3$ model was proposed for corundum with Al^{+3}, Fe^{+3} species mixed in the first sublattice, and the second sublattice is occupied by oxygen. For a two-sublattice model, the

Gibbs energy is given as

$$G^{\varphi}(\{y_i\},T) = \sum_i \sum_j y_i^{(1)} y_j^{(2)} G_{i:j} - TS^c + G^{ex} + G^{magn}, \quad (1)$$

where i and j are the atoms or ions, (1), (2) are the numbers of the sublattices, y are the site fractions of the atoms or ions in the sublattice, $G_{i:j}$ is the Gibbs energy of the end-member, T is the temperature, S^c is the configurational entropy, G^{ex} is the excess Gibbs energy, G^{magn} is the magnetic contribution to the Gibbs energy due to the magnetic ordering. The last one term is not required only for wüstite.

The S^c variable is defined as follows

$$S^c = -R\left[n_1 \sum_i y_i^{(1)} \ln y_i^{(1)} + n_2 \sum_j y_j^{(2)} \ln y_j^{(2)}\right], \quad (2)$$

here n is the stoichiometric number of each sublattice; R is the ideal gas constant.

The excess Gibbs energies of corundum and hematite, and wüstite were described with Redlich-Kister expressions: wüstite

$$G^{ex}_{hal}(\{y_i\},T) = y_{Fe^{+2}} y_{Fe^{+3}} ({}^0L^{hal}_{Fe^{+2},Fe^{+3}:O^{-2}} + {}^1L^{hal}_{Fe^{+2},Fe^{+3}:O^{-2}}(y_{Fe^{+2}} - y_{Fe^{+3}})) + y_{Al^{+3}} y_{Fe^{+3}} {}^0L^{hal}_{Al^{+3},Fe^{+3}:O^{-2}}), \quad (3)$$

corundum and hematite

$$G^{ex}_{cor}(\{y_i\},T) = y_{Al^{+3}} y_{Fe^{+3}} \left({}^0L^{cor}_{Al^{+3},Fe^{+3}:O^{-2}} + {}^1L^{cor}_{Al^{+3},Fe^{+3}:O^{-2}} \times (y_{Al^{+3}} - y_{Fe^{+3}})\right), \quad (4)$$

here ${}^0L^{hal}_{Fe^{+2},Fe^{+3}:O^{-2}}$, ${}^1L^{hal}_{Fe^{+2},Fe^{+3}:O^{-2}}$ are the interaction parameters for the binary Fe–O system and accepted according [13]; ${}^0L^{hal}_{Al^{+3},Fe^{+3}:O^{-2}}$, ${}^0L^{cor}_{Al^{+3},Fe^{+3}:O^{-2}}$, ${}^1L^{cor}_{Al^{+3},Fe^{+3}:O^{-2}}$ are the interaction parameters in the ternary Al–Fe–O system assessed in this work.

The magnetic contribution is expressed according to Inden [57], and Hillert and Jarl [58]

$$G^{magn}(\{y_i\},T) = RT \ln(\beta+1) f(\tau), \quad (5)$$

where τ is equal to T/T_{cr}; T_{cr} is the critical temperature for magnetic ordering; β is the average magnetic moment per atom in Bohr magnetons.

3.2. $Al_2Fe_2O_6$ compound

The Gibbs energy of the stoichiometric $Al_2Fe_2O_6$ compound is expressed by

$$^{\circ}G^{Al_2Fe_2O_6(T)} - H^{SER} = A + BT + CT\ln T + DT^2 + ET^{-1}, \quad (6)$$

where H^{SER} is the sum of the molar enthalpy of the elements in its reference state at 25 °C; A through E are the coefficients.

3.3. Spinel phase

A proper description of the spinel phase is quite complicated. The four sublattice model for spinel description was applied in Refs. [13,56] to reproduce the degree of inversion and extension of homogeneity range towards M_2O_3 and MO compositions, where M is metal. However, the selection of independent parameters and description of dependent parameters can be different [13,56,59] and must be described step by step. The following designations are accepted. Va stands for the vacancies. Letters "T" and "O" denote tetrahedral and octahedral lattice sites.

3.3.1. Stoichiometric spinel

In the ternary Al–Fe–O system, the spinel phase is based on two spinels, namely magnetite (Fe_3O_4) and hercynite ($FeAl_2O_4$). Firstly, we considered the stoichiometric $FeAl_2O_4$ phase. The oxygen ions form an fcc lattice in the spinel structure, and divalent and trivalent cations are distributed in the tetrahedral and octahedral sublattices. In the case of the normal spinel structure, the divalent ions occupy the tetrahedral sublattice, and the trivalent ions occupy the octahedral sublattice. In general, the expression $(Fe^{+2})^T(Al^{+3})^O_2O_4$ could be written for the normal spinel. If the trivalent cations occupy the tetrahedral sublattice while divalent and trivalent ions are mixed in the octahedral one in ratio 1:1, then the spinel structure is referred as inverse and could be denoted as $(Al^{+3})^T(Fe^{+2}_{0.5}Al^{+3}_{0.5})^O_2O_4$. For the inverse spinel, the electroneutrality reaction could be written as follows

$$\frac{1}{2}\left(Al^{+3}\right)^T\left(Al^{+3}\right)^O_2O_4 + \frac{1}{2}\left(Al^{+3}\right)^T\left(Fe^{+2}\right)^O_2O_4 = \left(Al^{+3}\right)^T\left(Fe^{+2}_{0.5}Al^{+3}_{0.5}\right)^O_2O_4. \quad (7)$$

Between these two cases, spinel solid solution presents different degree of inversion defined as site fraction of Al^{+3} in the first sublattice. To describe stoichiometric $FeAl_2O_4$ phase with different degrees of inversion, the four-sublattices formula $(Al^{+3}, Fe^{+2})_1(Al^{+3}, Fe^{+2})_2(Va)_2(O^{-2})_4$ was used. The first sublattice corresponds to the tetrahedral sites; the second and third sublattices represent the octahedral sites. The third sublattice is required to take into account a deviation from the stoichiometry towards excess of FeO. Sundman [13] accounted this small deviation in magnetite. In hercynite, homogeneity range extension towards FeO was not found. In the present work, we did not consider this particular case and simplified description [13]. However, the third sublattice is reserved for the future development of the model.

The Gibbs energy of the stoichiometric $FeAl_2O_4$ is as follows

$$G^{spin}(\{y_i\},T) = y^T_{Al^{+3}} y^O_{Al^{+3}} {}^{\circ}G_{Al^{+3}:Al^{+3}} + y^T_{Al^{+3}} y^O_{Fe^{+2}} {}^{\circ}G_{Al^{+3}:Fe^{+2}} + y^T_{Fe^{+2}} y^O_{Al^{+3}} {}^{\circ}G_{Fe^{+2}:Al^{+3}} + y^T_{Fe^{+2}} y^O_{Fe^{+2}} {}^{\circ}G_{Fe^{+2}:Fe^{+2}} + RT\left(y^T_{Al^{+3}} \ln y^T_{Al^{+3}} + y^T_{Fe^{+2}} \ln y^T_{Fe^{+2}} + 2\left(y^O_{Al^{+3}} \ln y^O_{Al^{+3}} + y^O_{Fe^{+2}} \ln y^O_{Fe^{+2}}\right)\right), \quad (8)$$

where ${}^{\circ}G_{Al^{+3}:Al^{+3}}$, ${}^{\circ}G_{Al^{+3}:Fe^{+2}}$, ${}^{\circ}G_{Fe^{+2}:Al^{+3}}$, ${}^{\circ}G_{Fe^{+2}:Fe^{+2}}$ are the Gibbs energies of hypothetical compounds (end-members). The expressions for the ${}^{\circ}G_{Fe^{+2}:Fe^{+2}}$ and ${}^{\circ}G_{Al^{+3}:Al^{+3}}$ parameters have been taken from Sundman [13], and Zienert and Fabrichnaya [60] correspondingly. The ${}^{\circ}G_{Fe^{+2}:Al^{+3}}$ and ${}^{\circ}G_{Al^{+3}:Fe^{+2}}$ parameters must be determined in the present work.

The relations between the ${}^{\circ}G_{Al^{+3}:Al^{+3}}$, ${}^{\circ}G_{Al^{+3}:Fe^{+2}}$, ${}^{\circ}G_{Fe^{+2}:Al^{+3}}$, ${}^{\circ}G_{Fe^{+2}:Fe^{+2}}$ end-members could be represented by a reciprocal square (Fig. 1). The end-points of the neutral line between ${}^{\circ}G_{Fe^{+2}:Al^{+3}}$ and the middle point of the line connecting ${}^{\circ}G_{Al^{+3}:Al^{+3}}$ and ${}^{\circ}G_{Al^{+3}:Fe^{+2}}$ correspond to the normal and inverse spinels. The ${}^{\circ}G_{Fe^{+2}:Al^{+3}}$ term corresponds to the Gibbs energy of the normal spinel and is represented as

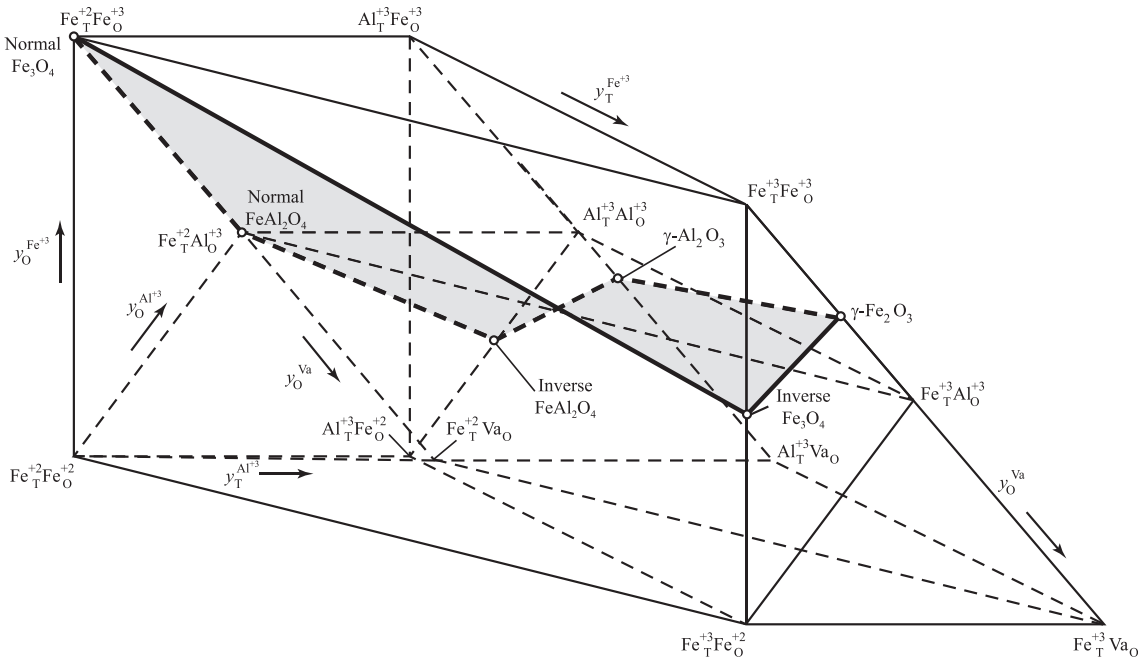

Fig. 1. Compositional space for spinel with a solubility of γ-Al_2O_3 and γ-Fe_2O_3. The bold solid and dashed lines represent neutral lines. The possible neutral planes are indicated with shaded regions.

Table 4
Thermodynamic parameters for the phases of the Al_2O_3–Fe_2O_3–FeO system. All values are given in SI units (J, mol^{-1}, K).

Model/parameters of the phase	Reference
IONIC_LIQUID: model $(Al^{+3},Fe^{+2})_P(O^{-2}, AlO_{1.5}, FeO_{1.5},Va)_Q$	
${}^0G^{IONIC\ LIQUID}_{AlO_{1.5}} = 0.5\ GAL2O3\_L$	[60]
${}^0G^{IONIC\ LIQUID}_{Al^{+3}:O^{-2}} = GAL2O3\_L + 1000000$	[60]
${}^oG_{Al}$=GALLIQ	[73]
${}^0G^{IONIC\ LIQUID}_{FeO_{1.5}} = -89819 + 39.962T + 2.5GFEOLIQ$	[13,63]
${}^0G^{IONIC\ LIQUID}_{Fe^{+2}:O^{-2}} = 4\ GFEOLIQ$	[13,63]
${}^\circ G_{Fe} = GFELIQ$	[73]
${}^0L^{IONIC\ LIQUID}_{Fe^{+2}:O^{-2},FeO_{1.5}} = -26362$	[13,63]
${}^1L^{IONIC\ LIQUID}_{Fe^{+2}:O^{-2},FeO_{1.5}} = 13353$	[13,63]
${}^0L^{IONIC\ LIQUID}_{Fe^{+2}:O^{-2},Va} = 176681-16.368T$	[13,63]
${}^1L^{IONIC\ LIQUID}_{Fe^{+2}:O^{-2},Va} = -65655 + 30.869T$	[13,63]
${}^0L^{IONIC\ LIQUID}_{Fe^{+2}:Va,FeO_{1.5}} = +110000$	[13,63]
${}^0L^{IONIC\ LIQUID}_{Al^{+3}:O^{-2},Va} = -829000 + 106T$	[64]
${}^0L^{IONIC\ LIQUID}_{Al^{+3}:Va,AlO_{1.5}} = +110000 + 46T$	[64]
${}^0L^{IONIC\ LIQUID}_{Al^{+3},Fe^{+2}:Va} = -88090 + 19.8T$	[65]
${}^1L^{IONIC\ LIQUID}_{Al^{+3},Fe^{+2}:Va} = -3800 + 3T$	[65]
${}^2L^{IONIC\ LIQUID}_{Al^{+3},Fe^{+2}:Va} = -2000$	[65]
${}^0L^{IONIC\ LIQUID}_{Fe^{+2}:O^{-2},AlO_{1.5}} = +188034 + 0.61T$	[7]
${}^0L^{IONIC\ LIQUID}_{Fe^{+2}:O^{-2},AlO_{1.5}} = 349303.91-186.22T$	This work
${}^1L^{IONIC\ LIQUID}_{Fe^{+2}:O^{-2},AlO_{1.5}} = 174253.98 - 83.76T$	This work
${}^0L^{IONIC\ LIQUID}_{Fe^{+2}:O^{-2},FeO_{1.5}AlO_{1.5}} = -610000$	This work
${}^1L^{IONIC\ LIQUID}_{Fe^{+2}:O^{-2},FeO_{1.5}AlO_{1.5}} = 1000$	This work
${}^2L^{IONIC\ LIQUID}_{Fe^{+2}:O^{-2},FeO_{1.5}AlO_{1.5}} = 1000$	This work
${}^0L^{IONIC\ LIQUID}_{AlO_{1.5},FeO_{1.5}} = 38407.84-1.47T$	This work
${}^1L^{IONIC\ LIQUID}_{AlO_{1.5},\ FeO_{1.5}} = 47635.61-32.09T$	This work

(*continued on next page*)

Table 4 (*continued*)

Model/parameters of the phase	Reference
Symbols	
GAL2O3_L ($298.15 < T < 600$) $= -1607850.8 + 405.559491T - 67.4804T\ln T - 0.06747T^2 + 1.4205433E\text{-}05T^3 + 938780T^{-1}$;	
GAL2O3_L ($600 < T < 1500$) $= -1625385.57 + 712.394972T - 116.258T\ln T - 0.0072257T^2 + 2.78532E\text{-}07T^3 + 2120700T^{-1}$;	
GAL2O3_L ($1500 < T < 1912$) $= -1672662.69 + 1010.9932T - 156.058T\ln T + 0.00709105T^2 - 6.29402E\text{-}07T^3 + 12366650T^{-1}$;	
GAL2O3_L ($1912 < T < 2327$) $= +29178041.6 - 168360.926T + 21987.1791T\ln T - 6.99552951T^2 + 4.10226192E\text{-}04T^3 - 7.98843618E + 09T^{-1}$;	
GAL2O3_L ($2327 < T < 4000$) $= -1757702.05 + 1344.84833T - 192.464T\ln T$.	
GALLIQ ($298.15 < T < 933.60$) $= +11005.553 - 11.840873T + 7.9401E\text{-}20T^7 +$ GHSERAL;	
GALLIQ ($933.60 < T < 6000$) $= +10481.974 - 11.252014T + 1.234264E + 28T^{-9} +$ GHSERAL.	
GHSERAL ($298.15 < T < 700$) $= -7976.15 + 137.093038T - 24.3671976T\ln T - .001884662T^2 - 8.77664E{-}07T^3 + 74092T^{-1}$;	
GHSERAL ($700 < T < 933.47$) $= -11276.24 + 223.048446T - 38.5844296T\ln T + 0.018531982T^2 - 5.764227E\text{-}06T^3 + 74092T^{-1}$;	
GHSERAL ($933.47 < T < 2900$) $= -11278.378 + 188.684153T - 31.748192T\ln T - 1.230524E + 28T^{-9}$.	
GFEOLIQ ($298.15 < T < 3000$) $= -137252 + 224.641T - 37.1815T\ln T$.	
GFELIQ ($298.15 < T < 1811$) $12040.17 - 6.55843T - 3.67516E{-}21T^7 +$ GHSERFE	
GFELIQ ($1811 < T < 6000$) $14544.751 - 8.01055T +$ GHSERFE-2.29603E $+ 31T^{-9}$.	
GHSERFE ($298.15 < T < 1811$) $= +1225.7 + 124.134T - 23.5143T\ln T - 0.00439752T^2 - 5.8927E\text{-}08T^3 + 77359T^{-1}$;	
GHSERFE ($1811 < T < 6000$) $= -25383.581 + 299.31255T - 46T\ln T + 2.29603E + 31T^{-9}$.	
CORUNDUM: model $(Al^{+3}, Fe^{+3})_2(O^{-2})_3$	
${}^0G^{CORUNDUM}_{Al^{+3}:O^{-2}} - 2H^{SER}_{Al} - 3H^{SER}_{O} =$ GCORUND	[56]
${}^0G^{CORUNDUM}_{Fe^{+3}:O^{-2}} - 2H^{SER}_{Fe} - 3H^{SER}_{O} =$ GFE2O3	[13]
$T^{CORUNDUM}_{0,cr\ Fe^{+3}:O^{-2}} = -2867$	[13]
$\beta^{CORUNDUM}_{0,cr_{Fe^{+3}:O^{-2}}} = -25.1$	[13]
${}^0L^{CORUNDUM}_{Al^{+3},Fe^{+3}:O^{-2}} = 95000 - 18.50T$	This work
${}^1L^{CORUNDUM}_{Al^{+3},Fe^{+3}:O^{-2}} = -11511.15 + 10T$	This work
Symbols	
GCORUND ($298.14 < T < 600$) $= -1707351.3 + 448.021092T - 67.4804T\ln T - 0.06747T^2 + 1.4205433E\text{-}05T^3 + 938780T^{-1}$;	
GCORUND ($600 < T < 1500$) $= -1724886.06 + 754.856573T - 116.258T\ln T - 0.0072257T^2 + 2.78532E\text{-}07T^3 + 2120700T^{-1}$;	
GCORUND ($1500 < T < 3000$) $= -1772163.19 + 1053.4548T - 156.058T\ln T + 0.00709105T^2 - 6.29402E\text{-}07T^3 + 12366650T^{-1}$.	
GFE2O3 ($298.15 < T < 3000$) $= -858683 + 827.946T - 137.0089T\ln T + 1453810T^{-1}$.	
HALITE: model $(Al^{+3}, Fe^{+2}, Fe^{+3}, Va)_1(O^{-2})_1$	
${}^0G^{HALITE}_{Al^{+3}:O^{-2}} - H^{SER}_{Al} - H^{SER}_{O} = 0.5$ GHALCORUND $- 0.5\ RT(2\ln 2 - 3\ln 3)$	[60]
${}^0G^{HALITE}_{Fe^{+2}:O^{-2}} - H^{SER}_{Fe} - H^{SER}_{O} =$ GWUSTITE	[13]
${}^0G^{HALITE}_{Fe^{+3}:O^{-2}} = 1.25$ AWUSTITE $+ 1.25$ GWUSTITE	[13]
${}^0L^{HALITE}_{Al^{+3},Fe^{+3}:O^{-2}} = 80.01T$	This work
${}^0L^{HALITE}_{Fe^{+2},Fe^{+3}:O^{-2}} = -12324$	[13]
${}^1L^{HALITE}_{Fe^{+2},Fe^{+3}:O^{-2}} = 20070$	[13]
Symbols	
GHALCORUND $=$ GCORUND $+ 143571.4 - 3T$	
GWUSTITE ($298.15 < T < 3000$) $= -279318 + 252.848T - 46.12826T\ln T - 0.0057402984T^2$.	
AWUSTITE ($298.15 < T < 3000$) $= -55384 + 27.888T$	
BCC_A2: model $(Fe,O)_1(Va)_3$	
${}^0G^{BCC\_A2}_{O:Va} - H^{SER}_{O} = 0.5$ GO2GAS $+ 30000$	[13]
${}^0G^{BCC\_A2}_{Fe:Va} - H^{SER}_{Fe} =$ GHSERFE	[13]
$T^{BCC\_A2}_{0,cr\ Fe:Va} = 1043$	[13]
$\beta^{BCC\_A2}_{0,cr\ Fe:Va} = 2.22$	[13]
${}^0L^{BCC\_A2}_{Fe,O:Va} = -209794 + 84T$	[13]
Symbols	
GO2GAS ($298.15 < T < 1000$) $= -6961.74451 - 76729.7484T^{-1} - 51.0057202T - 22.2710136T\ln T - 0.01019774697T^2 + 1.32369208E\text{-}06T^3$;	
GO2GAS ($1000 < T < 3300$) $= -13137.5203 + 525809.556T^{-1} + 25.3200332T - 33.627603T\ln T - 0.00119159274T^2 + 1.35611111E\text{-}08T^3$;	
GO2GAS ($3300 < T < 6000$) $= -27973.4908 + 8766421.4T^{-1} + 62.5195726T - 37.9072074T\ln T - 8.50483772E\text{-}04T^2 + 2.14409777E\text{-}08T^3$.	
FCC_A1: model $(Fe,O)_1(Va)_1$	
${}^0G^{FCC\_A1}_{O:Va} - H^{SER}_{O} = 0.5$ GO2GAS $+ 30000$	[13]
${}^0G^{FCC\_A1}_{Fe:Va} - H^{SER}_{Fe} =$ GFEFCC $+$ GPFEFCC	[13]
$T^{FCC\_A1}_{0,cr_{Fe:Va}} = -201$	[13]
$\beta^{FCC\_A1}_{0,cr_{Fe:Va}} = -2.1$	[13]
${}^0L^{FCC\_A1}_{Fe,O:Va} = -199345.5 + 84T$	[13]
Symbols	
GFEFCC ($298.15 < T < 1811$) $= -236.7 + 132.416T - 24.6643T\ln T - 0.00375752T^2 - 5.8927E\text{-}08T^3 + 77359T^{-1}$;	
GFEFCC ($1811 < T < 6000$) $= -27097.396 + 300.25256T - 46T\ln T + 2.78854E{+}31T^{-9}$.	
GPFEFCC($298.15 < T < 6000$) $= 0$	
FE2AL2O6: model $(Fe^{+3})_2(Al^{+3})_2(O^{-2})_6$	

Table 4 (*continued*)

Model/parameters of the phase	Reference
${}^{0}G^{FE2AL2O6}_{Fe^{+3}:Al^{+3}:O^{-2}} - 2H^{SER}_{Al} - 2H^{SER}_{Fe} - 6H^{SER}_{O} (298.15 < T < 3000) = -2574540 + 1604.26T - 253.22T\ln T - 0.026T^2 + 3003754.10T^{-1}$	This work
SPINEL: model $(Al^{+3}, Fe^{+2}, Fe^{+3})_1(Al^{+3}, Fe^{+2}, Fe^{+3}, Va)_2(Va)_2(O^{-2})_4$	
${}^{0}G^{SPINEL}_{Al^{+3}:Al^{+3}:Va:O^{-2}} - 3H^{SER}_{Al} - 4H^{SER}_{O} = GALAL$	[60]
${}^{0}G^{SPINEL}_{Al^{+3}:Va:Va:O^{-2}} - H^{SER}_{Al} - 4H^{SER}_{O} = 8\ GALGAMMA - 5\ GALAL - 2RT(5\ln5 - 6\ln6)$	[60]
${}^{0}G^{SPINEL}_{Al^{+3}:Fe^{+2}:Va:O^{-2}} - H^{SER}_{Al} - 2H^{SER}_{Fe} - 4H^{SER}_{O} = GALFE$	This work
${}^{0}G^{SPINEL}_{Al^{+3}:Fe^{+3}:Va:O^{-2}} - H^{SER}_{Al} - 2H^{SER}_{Fe} - 4H^{SER}_{O} = GALFE - B - 71136.19$	This work
${}^{0}G^{SPINEL}_{Fe^{+2}:Al^{+3}:Va:O^{-2}} - 2H^{SER}_{Al} - H^{SER}_{Fe} - 4H^{SER}_{O} = NSPINEL$	This work
${}^{0}G^{SPINEL}_{Fe^{+3}:Al^{+3}:Va:O^{-2}} - H^{SER}_{Fe} - 2H^{SER}_{Al} - 4H^{SER}_{O} = NSPINEL - B + 50030$	This work
${}^{0}G^{SPINEL}_{Fe^{+2}:Va:Va:O^{-2}} - H^{SER}_{Fe} - 4H^{SER}_{O} = 5\ G + C$	[13]
${}^{0}G^{SPINEL}_{Fe^{+3}:Va:Va:O^{-2}} - H^{SER}_{Fe} - 4H^{SER}_{O} = 5G + C - B$	[13]
${}^{0}G^{SPINEL}_{Fe^{+2}:Fe^{+2}:Va:O^{-2}} - 3H^{SER}_{Fe} - 4H^{SER}_{O} = 7\ G + B$	[13]
${}^{0}G^{SPINEL}_{Fe^{+3}:Fe^{+3}:Va:O^{-2}} - 3H^{SER}_{Fe} - 4H^{SER}_{O} = 7\ G - B$	[13]
${}^{0}G^{SPINEL}_{Fe^{+2}:Fe^{+3}:Va:O^{-2}} - 3H^{SER}_{Fe} - 4H^{SER}_{O} = 7\ G$	[13]
${}^{0}G^{SPINEL}_{Fe^{+3}:Fe^{+2}:Va:O^{-2}} - 3H^{SER}_{Fe} - 4H^{SER}_{O} = 7\ G$	[13]
${}^{0}L^{SPINEL}_{Al^{+3},Fe^{+2}:Al^{+3}:Va:O^{-2}} = 91928.63 - 8.10T$	This work
${}^{0}L^{SPINEL}_{Al^{+3}:Al^{+3},Fe^{+2}:Va:O^{-2}} = -47148.27$	This work
${}^{0}L^{SPINEL}_{Al^{+3},Fe^{+2}:Fe^{+2}:Va:O^{-2}} = 19660.93$	This work
${}^{0}L^{SPINEL}_{Fe^{+2}:Al^{+3},Fe^{+2}:Va:O^{-2}} = -7088.79 + 3.63T$	This work
${}^{0}L^{SPINEL}_{Al^{+3}:Fe^{+2},Va:Va:O^{-2}} = 400000$	This work
${}^{0}L^{SPINEL}_{Al^{+3}:Fe^{+3},Va:Va:O^{-2}} = 1000000$	This work
$T^{SPINEL}_{0,cr\ Fe^{+2}:Va:Va:O^{-2}} = T^{SPINEL}_{0,cr\ Fe^{+3}:Va:Va:O^{-2}} = T^{SPINEL}_{0,cr\ Fe^{+2}:Fe^{+2}:Va:O^{-2}} = T^{SPINEL}_{0,cr\ Fe^{+3}:Fe^{+3}:Va:O^{-2}} = T^{SPINEL}_{0,cr\ Fe^{+2}:Fe^{+3}:Va:O^{-2}} = T^{SPINEL}_{0,cr\ Fe^{+3}:Fe^{+2}:Va:O^{-2}} = 848$	[13]
$\beta^{SPINEL}_{0,cr\ Fe^{+2}:Va:Va:O^{-2}} = \beta^{SPINEL}_{0,cr\ Fe^{+3}:Va:Va:O^{-2}} = \beta^{SPINEL}_{0,cr\ Fe^{+2}:Fe^{+2}:Va:O^{-2}} = \beta^{SPINEL}_{0,cr\ Fe^{+3}:Fe^{+3}:Va:O^{-2}} = \beta^{SPINEL}_{0,cr\ Fe^{+2}:Fe^{+3}:Va:O^{-2}} = \beta^{SPINEL}_{0,cr\ Fe^{+3}:Fe^{+2}:Va:O^{-2}} = 44.54$	[13]
Symbols	
GALAL $(298.15 < T < 6000) = 1.5$ GCORUND $- 0.5$ GHSEROO	
GHSEROO $(298.15 < T < 1000) = -3480.87 - 25.503038T - 11.136T\ln T - 0.005098888T^2 + 6.61846E\text{-}07T^3 - 38365T^{-1}$;	
GHSEROO $(1000 < T < 3300) = -6568.763 + 12.65988T - 16.8138T\ln T - 5.95798E\text{-}04T^2 + 6.781E\text{-}09T^3 + 2629057T^{-1}$;	
GHSEROO $(3300 < T < 6000) = -13986.728 + 31.259625T - 18.9536T\ln T - 4.25243E\text{-}04T^2 + 1.0721E\text{-}08T^3 + 4383200T^{-1}$.	
GALGAMMA $(298.15 < T < 6000) =$ GCORUND $+ 27140.4693 - 11.3005T$	
GALFE $(298.15 < T < 6000) = 2$ ISPINEL $-$ GALAL $+ 4RT\ln2$	
ISPINEL $(298.15 < T < 3000) =$ NSPINEL$+145480.96 - 75.73T$	
NSPINEL $(298.15 < T < 3000) =$ FEAL2O4 $+ 26760.77 - 8.14T$	
FEAL2O4 $(298.15 < T < 6000) = -2038876.8 + 959.91444T - 155.3938T\ln T - 0.013075T^2 + 1566908T^{-1}$	
B $(298.15 < T < 3000) = 46826 - 27.266T$	
C $(298.15 < T < 3000) = 120730 - 20.102T$	
G $(298.15 < T < 3000) = -161731 + 144.873T - 24.9879T\ln T - 0.0011952256T^2 + 206520T^{-1}$	

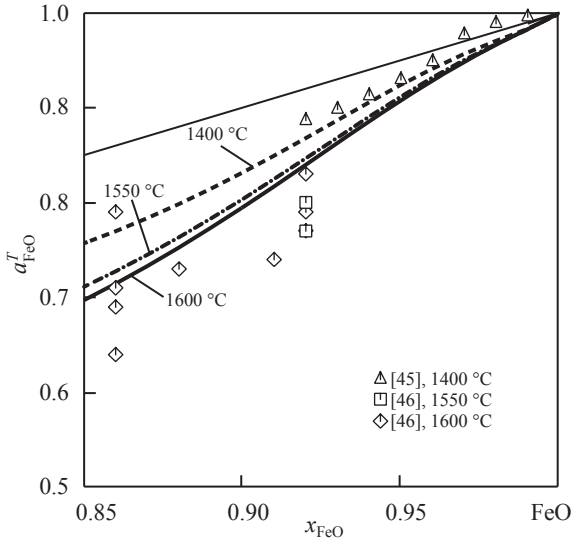

Fig. 2. Calculated activity of FeO in the liquid phase in comparison with experimental data. The standard reference state of FeO is a pure liquid component.

$$^{\circ}G_{Fe^{+2}:Al^{+3}} = \text{NSPINEL} = \text{FEAL2O4} + a_1, \quad (9)$$

here FEAL2O4 is the parameter related to the Gibbs energy of formation of hercynite, a_1 is the optimized parameter. According to Equation (7), the Gibbs energy of the inverse spinel could be given by the equation

$$^{\circ}G^{inv}\left(\{y^{Fe^{+2}}_{O} = 0.5, y^{Al^{+3}}_{O} = 0.5\}, T\right) = \text{ISPINEL} = \frac{1}{2}\left(^{\circ}G_{Al^{+3}:Fe^{+2}} + ^{\circ}G_{Al^{+3}:Al^{+3}} - 4RT\ln2\right), \quad (10)$$

with

$$\text{ISPINEL} = \text{NSPINEL} + a_2, \quad (11)$$

where a_2 is the optimized parameter.

The $^{\circ}G_{Al^{+3}:Fe^{+2}}$ parameter is determined by the reciprocal reaction

$$^{\circ}G_{Al^{+3}:Al^{+3}} + ^{\circ}G_{Fe^{+2}:Fe^{+2}} - G_{Al^{+3}:Fe^{+2}} - ^{\circ}G_{Fe^{+2}:Al^{+3}} = \Delta G_1. \quad (12)$$

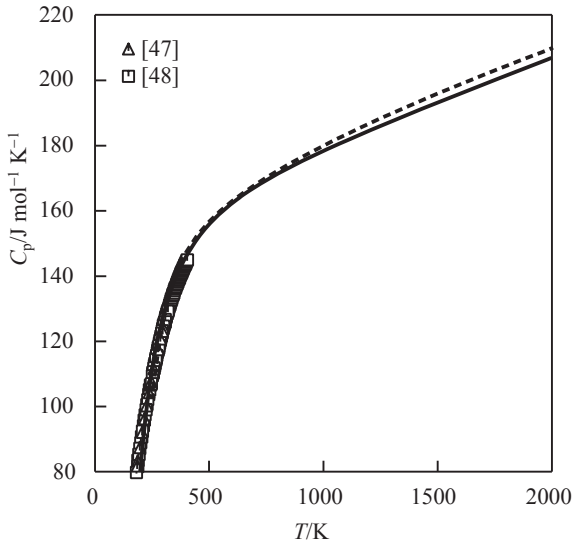

Fig. 3. The calculated heat capacity of hercynite. Continuous line is calculated according to this work. Dashed line is calculated according to the database for minerals [55]. Symbols correspond to experimental values.

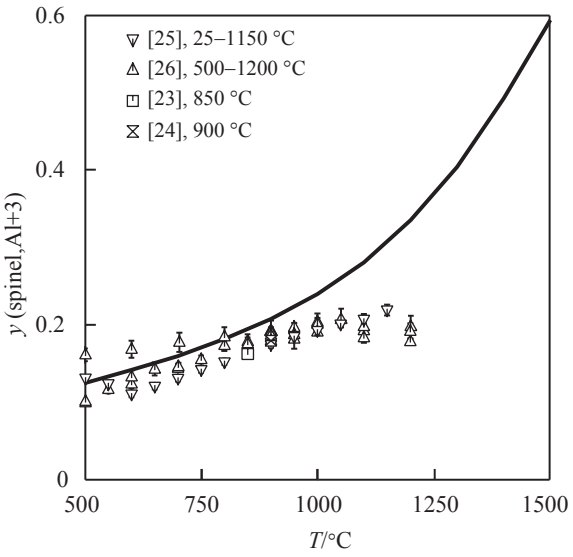

Fig. 4. Calculated amount of Al^{+3} cations on the first (tetragonal) sublattice in spinel phase (hercynite) (continuous line) and experimental values (symbols) at different temperatures.

Table 5
Calculated standard entropies and the enthalpy of formation of hercynite and $Al_2Fe_2O_6$ compound in comparison with literature data.[a]

$\Delta_f H_{298}$ in J mol^{-1}	S°_{298} in J K^{-1} mol^{-1}	Reference
Hercynite		
−1968000	108 ± 1	[43]
	106.3	[47]
	113.9	[48]
−1966000	106.27	[49]
−1956000	116 ± 0.8	[50]
−1951000	118.3	[51]
−1953000	116.9 ± 0.1	[52]
−1945000	123.1	[53]
−1959180	107.5	[54]
−1955000	117.024	[55]
−1954000	114.4	This work
$Al_2Fe_2O_6$		
55800	197.6	[44]
22400	141.4	This work

[a] For hercynite the enthalpy of formation from pure elements is given, the enthalpy of formation from oxides is given for $Al_2Fe_2O_6$ compound.

In our case, the ΔG_1 term is not equal to zero since the ${}^\circ G_{Al^{+3}:Al^{+3}}$, ${}^\circ G_{Fe^{+2}:Al^{+3}}$, ${}^\circ G_{Fe^{+2}:Fe^{+2}}$ parameters have definite values. For these reasons, the ${}^\circ G_{Al^{+3}:Fe^{+2}}$ term has been expressed from Equation (10)

$$ {}^\circ G_{Al^{+3}:Fe^{+2}} = \mathrm{GALFE} = 2\mathrm{ISPINEL} - {}^\circ G_{Al^{+3}:Al^{+3}} + 4RT\ln 2. \quad (13)$$

This term is used to model the degree of inversion. It should be noted that ΔG terms of reciprocal reactions are usually assumed to be zero at first, and then are used as optimizing parameters if it is not possible to reproduce experimental data with zero values.

Since all required parameters are defined for the hercynite, the next step is to include magnetite (Fe_3O_4) in the model of spinel. The Fe^{+3} cations should be introduced in the first and the second sublattices. Thus, the formula for the spinel is extended accordingly $(Al^{+3}, Fe^{+2}, Fe^{+3})_1(Al^{+3}, Fe^{+2}, Fe^{+3})_2(Va)_2(O^{-2})_4$. Graphically, this could be represented by three adjacent triangular prisms (Fig. 1). The Gibbs energy of the spinel is given by

$$\begin{aligned} G^{\mathrm{spin}}(\{y_i\},T) = {} & y^T_{Al^{+3}} y^O_{Al^{+3}} {}^\circ G_{Al^{+3}:Al^{+3}} + y^T_{Al^{+3}} y^O_{Fe^{+2}} {}^\circ G_{Al^{+3}:Fe^{+2}} \\ & + y^T_{Fe^{+2}} y^O_{Al^{+3}} {}^\circ G_{Fe^{+2}:Al^{+3}} + y^T_{Fe^{+2}} y^O_{Fe^{+2}} {}^\circ G_{Fe^{+2}:Fe^{+2}} \\ & + y^T_{Al^{+3}} y^O_{Fe^{+3}} {}^\circ G_{Al^{+3}:Fe^{+3}} + y^T_{Fe^{+2}} y^O_{Fe^{+3}} {}^\circ G_{Fe^{+2}:Fe^{+3}} \\ & + y^T_{Fe^{+3}} y^O_{Al^{+3}} {}^\circ G_{Fe^{+3}:Al^{+3}} + y^T_{Fe^{+3}} y^O_{Fe^{+2}} {}^\circ G_{Fe^{+3}:Fe^{+2}} \\ & + y^T_{Fe^{+3}} y^O_{Fe^{+3}} {}^\circ G_{Fe^{+3}:Fe^{+3}} + RT\left(y^T_{Al^{+3}} \ln y^T_{Al^{+3}}\right. \\ & + y^T_{Fe^{+2}} \ln y^T_{Fe^{+2}} + y^T_{Fe^{+3}} \ln y^T_{Fe^{+3}} + 2\left(y^O_{Al^{+3}} \ln y^O_{Al^{+3}}\right. \\ & \left. \left. + y^O_{Fe^{+2}} \ln y^O_{Fe^{+2}} + y^O_{Fe^{+3}} \ln y^O_{Fe^{+3}}\right)\right). \end{aligned} \quad (14)$$

Accordingly, the ${}^\circ G_{Fe^{+2}:Fe^{+3}}$ term describes the Gibbs energy of the normal Fe_3O_4, which is unstable at room temperature, and the ${}^\circ G_{Fe^{+3}:Fe^{+2}}$ term is needed to model the degree of inversion. This term is essential since magnetite is inverse spinel of $(Fe^{+3})^T(Fe^{+2}_{0.5}Fe^{+3}_{0.5})^O_2O_4$ type at room temperature. All other parameters are the Gibbs energies of the hypothetical compounds. The values for the ${}^\circ G_{Fe^{+2}:Fe^{+3}}$, ${}^\circ G_{Fe^{+3}:Fe^{+2}}$, ${}^\circ G_{Fe^{+3}:Fe^{+3}}$ parameters were taken from Ref. [13]. The reference state for charged pseudo-components proposed by Sundman [13] was also adopted in the present work

$$ {}^\circ G_{Fe^{+2}:Fe^{+3}} = {}^\circ G_{Fe^{+3}:Fe^{+2}}. \quad (15)$$

Thus, the ${}^\circ G_{Al^{+3}:Fe^{+3}}$ and ${}^\circ G_{Fe^{+3}:Al^{+3}}$ parameters are the only one, which should be defined. The unknown terms can be found from the following reciprocal reactions

$$ Al^{+3}Fe^{+2} + Fe^{+3}Fe^{+3} \leftrightarrow Fe^{+3}Fe^{+2} + Al^{+3}Fe^{+3}, \quad (16)$$

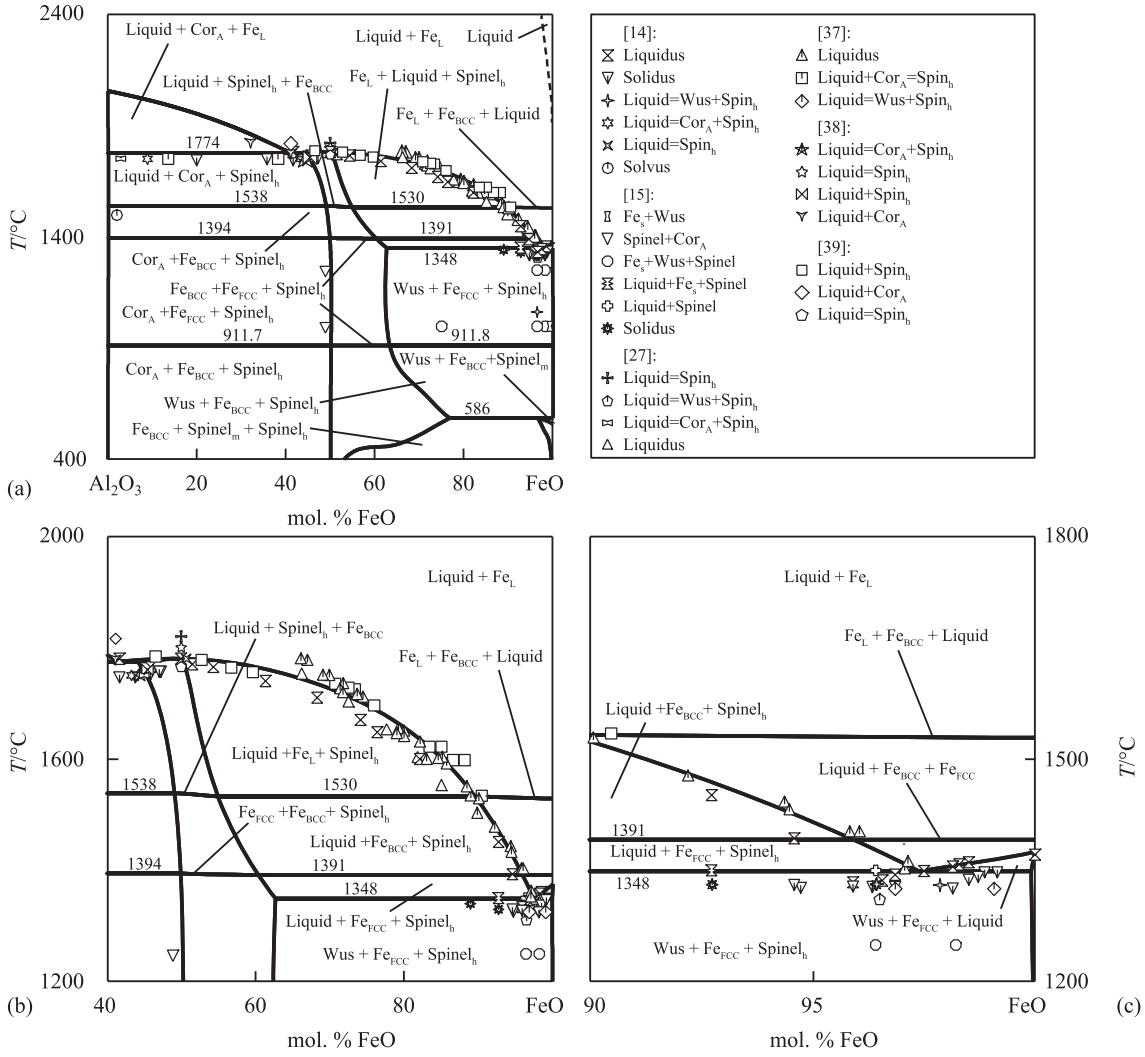

Fig. 5. A section from Al_2O_3 to FeO. Metallic iron is always present, in different modifications depending on the temperature: (a) overall view; (b) and (c) enlarged portions. Continuous lines are calculated phase boundaries according to this work; symbols correspond to experimental values. The designation "Fe_s" and "Fe_L" is given for solid and liquid iron.

$$Fe^{+2}Al^{+3} + Fe^{+3}Fe^{+3} \leftrightarrow Fe^{+2}Fe^{+3} + Fe^{+3}Al^{+3}, \quad (17)$$

$${}^{\circ}G_{Al^{+3}:Fe^{+3}} + {}^{\circ}G_{Fe^{+3}:Fe^{+2}} - G_{Al^{+3}:Fe^{+2}} - {}^{\circ}G_{Fe^{+3}:Fe^{+3}} = \Delta G_2, \quad (18)$$

$${}^{\circ}G_{Fe^{+2}:Fe^{+3}} + {}^{\circ}G_{Fe^{+3}:Al^{+3}} - G_{Fe^{+2}:Al^{+3}} - {}^{\circ}G_{Fe^{+3}:Fe^{+3}} = \Delta G_3. \quad (19)$$

where ΔG_2 and ΔG_3 are not equal to zero and must be optimized in the present work. The final equations as follows

$${}^{\circ}G_{Al^{+3}:Fe^{+3}} = GALFE - B + \Delta G_2, \quad (20)$$

$${}^{\circ}G_{Fe^{+3}:Al^{+3}} = NSPINEL - B + \Delta G_3. \quad (21)$$

here B is an additional coefficient in the Gibbs energies of end-members Fe^{+2}: Fe^{+2}:Va: O^{-2} and Fe^{+3}: Fe^{+3}:Va: O^{-2} determined by Sundman [13] for the binary Fe–O system.

3.3.2. Dissolution of Al_2O_3 and Fe_2O_3

The excess oxygen content in the spinel can be taken into account by the introducing of the vacancies in the octahedral sites. In this context, the formation of the γ modification of the Fe_2O_3 or Al_2O_3 oxide with a spinel related structure is assumed. The formula for the spinel is then given by $(Al^{+3}, Fe^{+2}, Fe^{+3})^T{}_1(Al^{+3}, Fe^{+2}, Fe^{+3}, Va)^O{}_2(Va)_2(O^{-2})_4$. This case is represented graphically in Fig. 1. Two new neutral end-points are found, which correspond to metastable γ-Fe_2O_3 and γ-Al_2O_3 phases. The Gibbs energy for the neutral end-point related to the metastable γ-Fe_2O_3 is accepted according [13]. For Al-rich and Fe-rich spinels, there are neutral planes within the prisms. The following electroneutrality reactions could be written for the dissolution of γ-Al_2O_3

$$\frac{5}{6}(Al^{+3})^T(Al^{+3})^O_2O_4 + \frac{1}{6}(Al^{+3})^T(Va)^O_2O_4 = (Al^{+3})^T\left(Al^{+3}_{\frac{5}{6}}Va_{\frac{1}{6}}\right)^O_2O_4. \quad (22)$$

The Gibbs energy of the spinel phase is

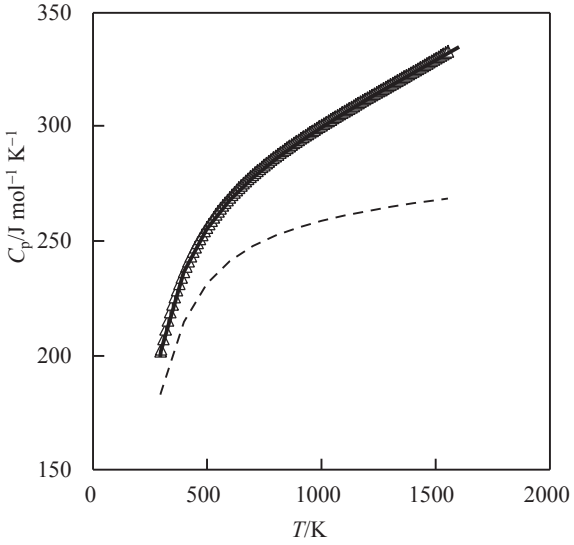

Fig. 6. The calculated heat capacity of $Al_2Fe_2O_6$ compound. Continuous line is the result of calculations according to this work. Dashed-dot line is calculated according to the Neumann-Kopp equation. Symbols correspond to experimental values [44].

$$
\begin{aligned}
G^{\text{spin}}(\{y_i\},T) = {} & y^{T}_{Al^{+3}} y^{O}_{Al^{+3}} {}^{\circ}G_{Al^{+3}:Al^{+3}} + y^{T}_{Al^{+3}} y^{O}_{Fe^{+2}} {}^{\circ}G_{Al^{+3}:Fe^{+2}} \\
& + y^{T}_{Fe^{+2}} y^{O}_{Al^{+3}} {}^{\circ}G_{Fe^{+2}:Al^{+3}} + y^{T}_{Fe^{+2}} y^{O}_{Fe^{+2}} {}^{\circ}G_{Fe^{+2}:Fe^{+2}} \\
& + y^{T}_{Al^{+3}} y^{O}_{Fe^{+3}} {}^{\circ}G_{Al^{+3}:Fe^{+3}} + y^{T}_{Fe^{+2}} y^{O}_{Fe^{+3}} {}^{\circ}G_{Fe^{+2}:Fe^{+3}} \\
& + y^{T}_{Fe^{+3}} y^{O}_{Al^{+3}} {}^{\circ}G_{Fe^{+3}:Al^{+3}} + y^{T}_{Fe^{+3}} y^{O}_{Fe^{+2}} {}^{\circ}G_{Fe^{+3}:Fe^{+2}} \\
& + y^{T}_{Fe^{+3}} y^{O}_{Fe^{+3}} {}^{\circ}G_{Fe^{+3}:Fe^{+3}} + y^{T}_{Al^{+3}} y^{O}_{Va} {}^{\circ}G_{Al^{+3}:Va} \\
& + y^{T}_{Fe^{+2}} y^{O}_{Va} {}^{\circ}G_{Fe^{+2}:Va} + y^{T}_{Fe^{+3}} y^{O}_{Va} {}^{\circ}G_{Fe^{+3}:Va} \\
& + RT\Big(y^{T}_{Al^{+3}} \ln y^{T}_{Al^{+3}} + y^{T}_{Fe^{+2}} \ln y^{T}_{Fe^{+2}} \\
& + y^{T}_{Fe^{+3}} \ln y^{T}_{Fe^{+3}} + 2\Big(y^{O}_{Al^{+3}} \ln y^{O}_{Al^{+3}} + y^{O}_{Fe^{+2}} \ln y^{O}_{Fe^{+2}} \\
& + y^{O}_{Fe^{+3}} \ln y^{O}_{Fe^{+3}} + y^{O}_{Va} \ln y^{O}_{Va}\Big)\Big),
\end{aligned}
\tag{23}
$$

here ${}^{\circ}G_{Al^{+3}:Va}$, ${}^{\circ}G_{Fe^{+2}:Va}$, ${}^{\circ}G_{Fe^{+3}:Va}$ are the Gibbs energies of the hypothetical compounds. The expressions for these parameters were taken from Ref. [60] (for ${}^{\circ}G_{Al^{+3}:Va}$) and [13] (for ${}^{\circ}G_{Fe^{+2}:Va}$, ${}^{\circ}G_{Fe^{+3}:Va}$). The Gibbs energy for the neutral end-point $((Al^{+3})^{T}(Al^{+3}_{\frac{5}{6}}Va_{\frac{1}{6}})^{O}_{2}O_4)$ is given by

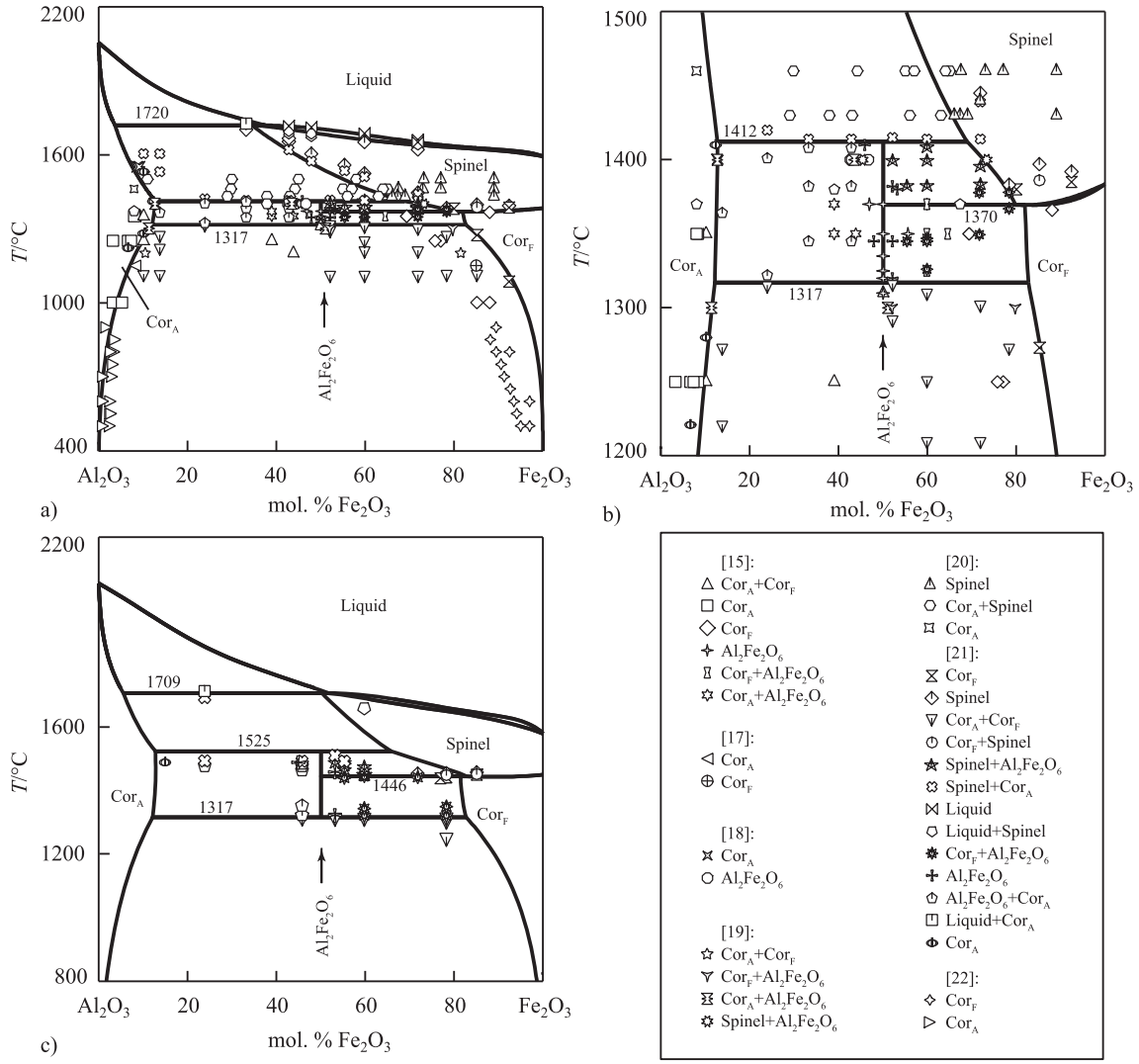

Fig. 7. Calculated Al_2O_3–Fe_2O_3 section of the Al_2O_3–Fe_2O_3–FeO system: (a) overall view at $p_{O_2} = 0.21$ atm; (b) enlarged portion at $p_{O_2} = 0.21$ atm; (c) overall view at $p_{O_2} = 1$ atm. Continuous lines are calculated phase boundaries according to this work; symbols correspond to experimental values.

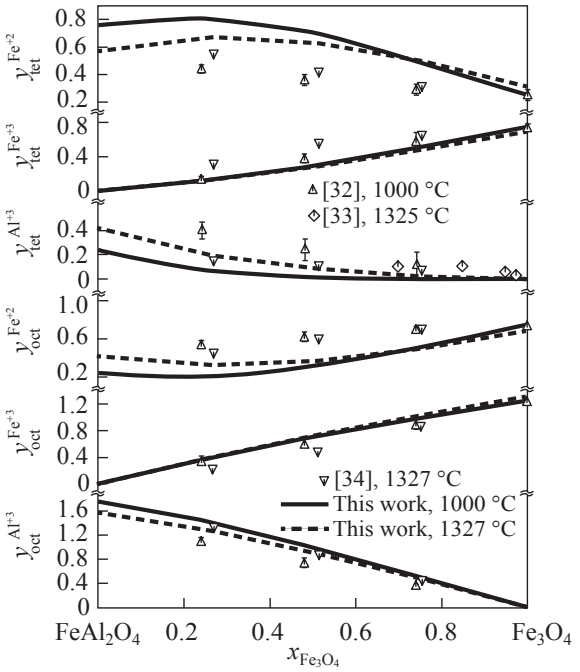

Fig. 8. Calculated amount of cations on the first (tetragonal) and second (octahedral) sublattices in spinel phase along the section $FeAl_2O_4$–Fe_3O_4 at different temperatures. Continuous lines are the results of calculations according to this work; symbols correspond to experimental values.

$$^{\circ}G^{\gamma-Al_2O_3}\left(\{y^{O}_{Va}=\frac{1}{6},y^{O}_{Al^{+3}}=\frac{5}{6}\},,T\right)=\frac{4}{3}\mathrm{GGAMMA}$$
$$=\frac{1}{6}\left(5\,^{\circ}G_{Al^{+3}:Al^{+3}}+\,^{\circ}G_{Al^{+3}:Va}-2RT(6\ln 6-5\ln 5)\right). \quad (24)$$

The interaction parameters are also considered in the present model to suppress spinel decomposition at higher temperatures and compensate large negative contribution from the $^{\circ}G_{Al^{+3}:Va}$ parameter. The equation for the spinel phase is as follows

$$\begin{aligned}G^{spin}(\{y_i\},T)=&\,y^{T}_{Al^{+3}}y^{O}_{Al^{+3}}\,^{\circ}G_{Al^{+3}:Al^{+3}}+y^{T}_{Al^{+3}}y^{O}_{Fe^{+2}}\,^{\circ}G_{Al^{+3}:Fe^{+2}}\\&+y^{T}_{Fe^{+2}}y^{O}_{Al^{+3}}\,^{\circ}G_{Fe^{+2}:Al^{+3}}+y^{T}_{Fe^{+2}}y^{O}_{Fe^{+2}}\,^{\circ}G_{Fe^{+2}:Fe^{+2}}\\&+y^{T}_{Al^{+3}}y^{O}_{Fe^{+3}}\,^{\circ}G_{Al^{+3}:Fe^{+3}}+y^{T}_{Fe^{+2}}y^{O}_{Fe^{+3}}\,^{\circ}G_{Fe^{+2}:Fe^{+3}}\\&+y^{T}_{Fe^{+3}}y^{O}_{Al^{+3}}\,^{\circ}G_{Fe^{+3}:Al^{+3}}+y^{T}_{Fe^{+3}}y^{O}_{Fe^{+2}}\,^{\circ}G_{Fe^{+3}:Fe^{+2}}\\&+y^{T}_{Fe^{+3}}y^{O}_{Fe^{+3}}\,^{\circ}G_{Fe^{+3}:Fe^{+3}}+y^{T}_{Al^{+3}}y^{O}_{Va}\,^{\circ}G_{Al^{+3}:Va}\\&+y^{T}_{Fe^{+2}}y^{O}_{Va}\,^{\circ}G_{Fe^{+2}:Va}+y^{T}_{Fe^{+3}}y^{O}_{Va}\,^{\circ}G_{Fe^{+3}:Va}\\&+RT\left(y^{T}_{Al^{+3}}\ln y^{T}_{Al^{+3}}+y^{T}_{Fe^{+2}}\ln y^{T}_{Fe^{+2}}+y^{T}_{Fe^{+3}}\ln y^{T}_{Fe^{+3}}\right.\\&+2\left(y^{O}_{Al^{+3}}\ln y^{O}_{Al^{+3}}+y^{O}_{Fe^{+2}}\ln y^{O}_{Fe^{+2}}+y^{O}_{Fe^{+3}}\ln y^{O}_{Fe^{+3}}\right.\\&\left.\left.+y^{O}_{Va}\ln y^{O}_{Va}\right)\right)+y^{T}_{Al^{+3}}y^{T}_{Fe^{+2}}y^{O}_{Al^{+3}}\,^{0}L_{Al^{+3},Fe^{+2}:Al^{+3}}\\&+y^{T}_{Al^{+3}}y^{O}_{Al^{+3}}y^{O}_{Fe^{+2}}\,^{0}L_{Al^{+3}:Al^{+3},Fe^{+2}}\\&+y^{T}_{Fe^{+2}}y^{O}_{Al^{+3}}y^{O}_{Fe^{+2}}\,^{0}L_{Fe^{+2}:Al^{+3},Fe^{+2}}\\&+y^{T}_{Al^{+3}}y^{T}_{Fe^{+2}}y^{O}_{Fe^{+2}}\,^{0}L_{Al^{+3},Fe^{+2}:Fe^{+2}}\\&+y^{T}_{Al^{+3}}y^{O}_{Fe^{+2}}y^{O}_{Va}\,^{0}L_{Al^{+3}:Fe^{+2},Va}\\&+y^{T}_{Al^{+3}}y^{O}_{Fe^{+3}}y^{O}_{Va}\,^{0}L_{Al^{+3}:Fe^{+3},Va}.\end{aligned} \quad (25)$$

All required interaction parameters were assessed in the present work.

There is a magnetic transition in magnetite. Thus, the magnetic contribution to the Gibbs energy due to the magnetic ordering should be taken into account. The final expression for the Gibbs energy of the spinel is given by

$$G^{spin}_{fin}(\{y_i\},T)=G^{spin}(\{y_i\},T)+G_{magn}. \quad (26)$$

The Equation (5) is used for the description of the magnetic contribution. The values of the critical temperatures and magnetic moments were accepted according to [13]. It should be noted that there is no magnetic contribution from the end-members containing aluminum (for example, $Al^{+3}Fe^{+2}$, $Al^{+3}Fe^{+2}$ etc.).

3.4. Liquid

The liquid phase was described using the ionic liquid model [61,62]. The two-sublattice model given by the expression $(Al^{+3}, Fe^{+2})_P(O^{-2}, AlO_{1.5}, FeO_{1.5}, Va)_Q$ was used. P and Q are the numbers of sites on each sublattice. These variables vary to keep electroneutrality. The Gibbs energy of the phase is expressed as follows

$$\begin{aligned}G^{ion}(\{y_i\},T)=&\,y_{Al^{+3}}y_{O^{-2}}\,^{\circ}G_{Al^{+3}:O^{-2}}+y_{Fe^{+2}}y_{O^{-2}}\,^{\circ}G_{Fe^{+2}:O^{-2}}+\\&Q\left(y_{FeO_{1.5}}\,^{\circ}G_{FeO_{1.5}}+y_{AlO_{1.5}}\,^{\circ}G_{AlO_{1.5}}+y_{Al^{+3}}y_{Va}\,^{\circ}G_{Al}\right.\\&\left.+y_{Fe^{+2}}y_{Va}\,^{\circ}G_{Fe}\right)+RTP(y_{Al^{+3}}\ln y_{Al^{+3}}+y_{Fe^{+2}}\ln y_{Fe^{+2}})\\&+RTQ(y_{O^{-2}}\ln y_{O^{-2}}+y_{Va}\ln y_{Va}+y_{FeO_{1.5}}\ln y_{FeO_{1.5}}\\&+y_{AlO_{1.5}}\ln y_{AlO_{1.5}})+G^{ex}_{ion}(\{y_i\},T),\end{aligned} \quad (27)$$

here $G^{ex}_{ion}(\{y_i\},T)$ is the excess Gibbs energy that depends on the interaction of the species in each sublattice. The expression for the $G^{ex}_{ion}(\{y_i\},T)$ function is given by

$$\begin{aligned}G^{ex}_{ion}(\{y_i\},T)=&\,y_{Fe^{+2}}y_{O^{-2}}y_{FeO_{1.5}}\left(^{0}L^{ion}_{Fe^{+2}:O^{-2},FeO_{1.5}}\right.\\&\left.+\,^{1}L^{ion}_{Fe^{+2}:O^{-2},FeO_{1.5}}(y_{O^{-2}}-y_{FeO_{1.5}})\right)\\&+Qy_{Al^{+3}}y_{Fe^{+2}}y^{2}_{Va}\left(^{0}L^{ion}_{Al^{+3},Fe^{+2}:Va}\right.\\&+\,^{1}L^{ion}_{Al^{+3},Fe^{+2}:Va}(y_{Al^{+3}}-y_{Fe^{+2}})\\&\left.+\,^{2}L^{ion}_{Al^{+3},Fe^{+2}:Va}(y_{Al^{+3}}-y_{Fe^{+2}})^{2}\right)\\&+y_{Al^{+3}}y_{O^{-2}}y_{Va}\,^{0}L^{ion}_{Al^{+3}:O^{-2},Va}\\&+Qy_{Al^{+3}}y_{Va}y_{AlO_{1.5}}\,^{0}L^{ion}_{Al^{+3}:Va,AlO_{1.5}}\\&+y_{Fe^{+2}}y_{O^{-2}}y_{Va}\left(^{0}L^{ion}_{Fe^{+2}:O^{-2},Va}+\,^{1}L^{ion}_{Fe^{+2}:O^{-2},Va}(y_{O^{-2}}\right.\\&\left.-y_{Va})\right)+Qy_{Fe^{+2}}y_{Va}y_{FeO_{1.5}}\,^{0}L^{ion}_{Fe^{+2}:Va,FeO_{1.5}}\\&+y_{Fe^{+2}}y_{O^{-2}}y_{AlO_{1.5}}\left(^{0}L^{ion}_{Fe^{+2}:O^{-2},AlO_{1.5}}\right.\\&\left.+\,^{1}L^{ion}_{Fe^{+2}:O^{-2},AlO_{1.5}}(y_{O^{-2}}-y_{AlO_{1.5}})\right)\\&+y_{Fe^{+2}}y_{O^{-2}}y_{FeO_{1.5}}y_{AlO_{1.5}}\left(^{0}L^{ion}_{Fe^{+2}:O^{-2},AlO_{1.5},FeO_{1.5}}\right.\\&+\,^{1}L^{ion}_{Fe^{+2}:O^{-2},AlO_{1.5},FeO_{1.5}}(y_{O^{-2}}-y_{AlO_{1.5}}-y_{FeO_{1.5}})\\&\left.+\,^{2}L^{ion}_{Fe^{+2}:O^{-2},AlO_{1.5},FeO_{1.5}}(y_{O^{-2}}-y_{AlO_{1.5}}-y_{FeO_{1.5}})^{2}\right)\\&+Qy_{Fe^{+2}}y_{Va}y_{AlO_{1.5}}\,^{0}L^{ion}_{Fe^{+2}:Va,AlO_{1.5}}\\&+Qy_{FeO_{1.5}}y_{AlO_{1.5}}\left(^{0}L^{ion}_{AlO_{1.5},FeO_{1.5}}\right.\\&\left.+\,^{1}L^{ion}_{AlO_{1.5},FeO_{1.5}}(y_{FeO_{1.5}}-y_{AlO_{1.5}})\right).\end{aligned} \quad (28)$$

Table 6
Invariant reactions in the Al_2O_3–Fe_2O_3 section at $p_{O_2} = 1$ atm.

Liquid + Cor_A ↔ Spinel							
T/°C	Liquid		Cor_A		Spinel		Reference
	mol.% Al_2O_3	mol.% Fe_2O_3	mol.% Al_2O_3	mol.% Fe_2O_3	mol.% Al_2O_3	mol.% Fe_2O_3	
1709	39	61	94.5	5.5	40	60	This work
Spinel + Cor_A ↔ $Al_2Fe_2O_6$							
T/°C	Cor_A		$Al_2Fe_2O_6$		Spinel		Reference
	mol.% Al_2O_3	mol.% Fe_2O_3	mol.% Al_2O_3	mol.% Fe_2O_3	mol.% Al_2O_3	mol.% Fe_2O_3	
1490	85	15			33	67	[21]
1525	87.3	12.7	50.0	50.0	40.8	59.2	This work
Spinel ↔ $Al_2Fe_2O_6$ + Cor_F							
T/°C	Spinel		$Al_2Fe_2O_6$		Cor_F		Reference
	mol.% Al_2O_3	mol.% Fe_2O_3	mol.% Al_2O_3	mol.% Fe_2O_3	mol.% Al_2O_3	mol.% Fe_2O_3	
1440	26	74			23	77	[21]
1446	19.8	80.2	50.0	50.0	18.6	81.4	This work
$Al_2Fe_2O_6$ ↔ Cor_F + Cor_A							
T/°C	$Al_2Fe_2O_6$		Cor_F		Cor_A		Reference
	mol.% Al_2O_3	mol.% Fe_2O_3	mol.% Al_2O_3	mol.% Fe_2O_3	mol.% Al_2O_3	mol.% Fe_2O_3	
1317	50.0	50.0	17.4	82.6	87.9	12.1	This work

Table 7
Invariant reactions for the Al_2O_3–Fe_2O_3 section at $p_{O_2} = 0.21$ atm.

Liquid + Cor_A ↔ Spinel							
T/°C	Liquid		Cor_A		Spinel		Reference
	mol.% Al_2O_3	mol.% Fe_2O_3	mol.% Al_2O_3	mol.% Fe_2O_3	mol.% Al_2O_3	mol.% Fe_2O_3	
1720	62.5	37.5	96.3	3.7	65.5	34.5	This work
Spinel + Cor_A ↔ $Al_2Fe_2O_6$							
T/°C	Cor_A		$Al_2Fe_2O_6$		Spinel		Reference
	mol.% Al_2O_3	mol.% Fe_2O_3	mol.% Al_2O_3	mol.% Fe_2O_3	mol.% Al_2O_3	mol.% Fe_2O_3	
1410	88	12			27	73	[21]
1412	87.3	12.7	50.0	50.0	31.1	68.9	This work
Spinel ↔ $Al_2Fe_2O_6$ + Cor_F							
T/°C	Spinel		$Al_2Fe_2O_6$		Cor_F		Reference
	mol.% Al_2O_3	mol.% Fe_2O_3	mol.% Al_2O_3	mol.% Fe_2O_3	mol.% Al_2O_3	mol.% Fe_2O_3	
1380	23	77			20	80	[21]
1370	20.7	79.3	50.0	50.0	20.2	79.8	This work
$Al_2Fe_2O_6$ ↔ Cor_F + Cor_A							
T/°C	$Al_2Fe_2O_6$		Cor_F		Cor_A		Reference
	mol.% Al_2O_3	mol.% Fe_2O_3	mol.% Al_2O_3	mol.% Fe_2O_3	mol.% Al_2O_3	mol.% Fe_2O_3	
1320							[15]
1318							[36]
1317	50.0	50.0	17.4	82.6	87.9	12.1	This work

Table 8
Invariant reactions in the ternary Al_2O_3–Fe_2O_3–FeO system in the presence of iron. The compositions are given in molar percent.

Liquid ↔ Spinel + Fe_L[a]								
Reference	T/°C (type)	Liquid			Spinel			p_{O_2}/atm.
		Al_2O_3	Fe_2O_3	FeO	Al_2O_3	Fe_2O_3	FeO	
[14] [b]	1780				50		50	
[27] [b]	1820 ± 15							
[38] [b]	1800							
[39] [b]	1765 ± 15							
This work	1780 (e_1, max)	50.2	0.4	49.4	50.9	0.2	48.9	$4.5 \cdot 10^{-9}$

(*continued on next page*)

Table 8 (*continued*)

Liquid ↔ Cor_A + Fe_L + Spinel/Liquid + Cor_A + Fe_L ↔ Spinel											
Reference	*T*/°C (type)	Liquid			Cor_A			Spinel			p_{O_2}/atm.
		Al_2O_3	Fe_2O_3	FeO	Al_2O_3	Fe_2O_3	FeO	Al_2O_3	Fe_2O_3	FeO	
[14] [b,c]	1750	57					9	55.8		44.2	
[27] [b,c]	1750 ± 15	55		45							
[37] [b,d]	1750										
[38] [b,c]	1750	56		44							
This work	1774 (P_1)	59	0.2	40.8	99.97	0.03	0	56	0.1	43.9	$2.2 \cdot 10^{-9}$
Fe_L + Cor_A ↔ BCC + Spinel											
Reference	*T*/°C (type)	Cor_A					Spinel				p_{O_2}/atm.
		Al_2O_3	Fe_2O_3	FeO			Al_2O_3	Fe_2O_3	FeO		
This work	1538 (U_1)	99.96	0.04	0			51.1	0.1	48.8		$7.4 \cdot 10^{-11}$
Fe_L + Spinel ↔ BCC + Liquid											
Reference	*T*/°C (type)	Cor_A					Spinel				p_{O_2}/atm.
		Al_2O_3	Fe_2O_3	FeO			Al_2O_3	Fe_2O_3	FeO		
This work	1530 (U_2)	11.8	6.8	81.4			47.4	2.6	50.0		$1.2 \cdot 10^{-9}$
BCC + Spinel ↔ FCC + Cor_A											
Reference	*T*/°C (type)	Spinel					Cor_A				p_{O_2}/atm.
		Al_2O_3	Fe_2O_3	FeO			Al_2O_3	Fe_2O_3	FeO		
This work	1394 (U_3)	50.3	0.1	49.6			99.96	0.04	0		$4.5 \cdot 10^{-12}$
Liquid + FCC ↔ Spinel + BCC											
Reference	*T*/°C (type)	Liquid					Spinel				p_{O_2}/atm.
		Al_2O_3	Fe_2O_3	FeO			Al_2O_3	Fe_2O_3	FeO		
This work	1391 (U_4)	4.6	7.6	87.8			44.3	5.7	50.0		$1.4 \cdot 10^{-10}$
Liquid + FCC ↔ Wüstite + Spinel											
Reference	*T*/°C (type)	Liquid			Wüstite			Spinel			p_{O_2}/atm.
		Al_2O_3	Fe_2O_3	FeO	Al_2O_3	Fe_2O_3	FeO	Al_2O_3	Fe_2O_3	FeO	
[14] [b]	1330	3.6			2						
[15]					1.3						
[27] [b]	1310 ± 10										
[37] [b]	1325										
This work	1348 (U_5)	2.8	7.1	90.1	0.1	5.2	94.7	42.8	7.2	50.0	$5.8 \cdot 10^{-11}$
Liquid ↔ Wüstite + Spinel											
Reference	*T*/°C (type)	Liquid			Wüstite			Spinel			p_{O_2}/atm.
		Al_2O_3	Fe_2O_3	FeO	Al_2O_3	Fe_2O_3	FeO	Al_2O_3	Fe_2O_3	FeO	
This work	1338 (e_5, min)	4.0	13.0	83.0	0	12.4	87.8	28.9	21.1	50.0	$1.6 \cdot 10^{-9}$
FCC + Wüstite ↔ BCC + Spinel											
Reference	*T*/°C (type)	Wüstite					Spinel				p_{O_2}/atm.
		Al_2O_3	Fe_2O_3	FeO			Al_2O_3	Fe_2O_3	FeO		
This work	911.8 (U_6)	0.01	5.19	94.8			42.3	7.7	50.0		$3.3 \cdot 10^{-17}$
FCC + Spinel ↔ BCC + Cor_A											
Reference	*T*/°C (type)	Spinel					Cor_A				p_{O_2}/atm.
		Al_2O_3	Fe_2O_3	FeO			Al_2O_3	Fe_2O_3	FeO		
This work	911.7 (U_7)	49.94	0.06	50.0			99.99	0.01	0		$4.5 \cdot 10^{-12}$
Wüstite + $Spinel_h$ ↔ $Spinel_m$ + BCC											
Reference	*T*/°C (type)	Wüstite			$Spinel_h$			$Spinel_m$			p_{O_2}/atm.
		Al_2O_3	Fe_2O_3	FeO	Al_2O_3	Fe_2O_3	FeO	Al_2O_3	Fe_2O_3	FeO	
This work	586 (U_8)	0	5.8	94.2	31.7	18.3	50	6.5	43.5	50.0	$5.2 \cdot 10^{-26}$

[a] The designation "Fe_L" is given for liquid iron.
[b] The compositions and temperatures are given for the Al_2O_3–FeO section in equilibrium with iron.
[c] The reaction is interpreted as an eutectic one.
[d] The reaction is interpreted as a peritectic one.

here ${}^0L^{ion}_{Fe^{+2}:O^{-2},FeO_{1.5}}$, ${}^1L^{ion}_{Fe^{+2}:O^{-2},FeO_{1.5}}$, ${}^0L^{ion}_{Fe^{+2}:O^{-2},Va}$, ${}^1L^{ion}_{Fe^{+2}:O^{-2},Va}$, and ${}^0L^{ion}_{Fe^{+2}:Va,FeO_{1.5}}$ are the interaction parameters for the binary Fe–O system [13,63]. ${}^0L^{ion}_{Al^{+3}:O^{-2},Va}$ and ${}^0L^{ion}_{Al^{+3}:Va,AlO_{1.5}}$ parameters in the Al–O system are accepted from Ref. [64]. ${}^0L^{ion}_{Al^{+3},Fe^{+2}:Va}$, ${}^1L^{ion}_{Al^{+3},Fe^{+2}:Va}$, and ${}^2L^{ion}_{Al^{+3},Fe^{+2}:Va}$ parameters are accepted from Ref. [65]. ${}^0L^{ion}_{Fe^{+2}:O^{-2},AlO_{1.5}}$ parameter is taken according to [7]. All other interaction parameters related to the ternary system are assessed in this work.

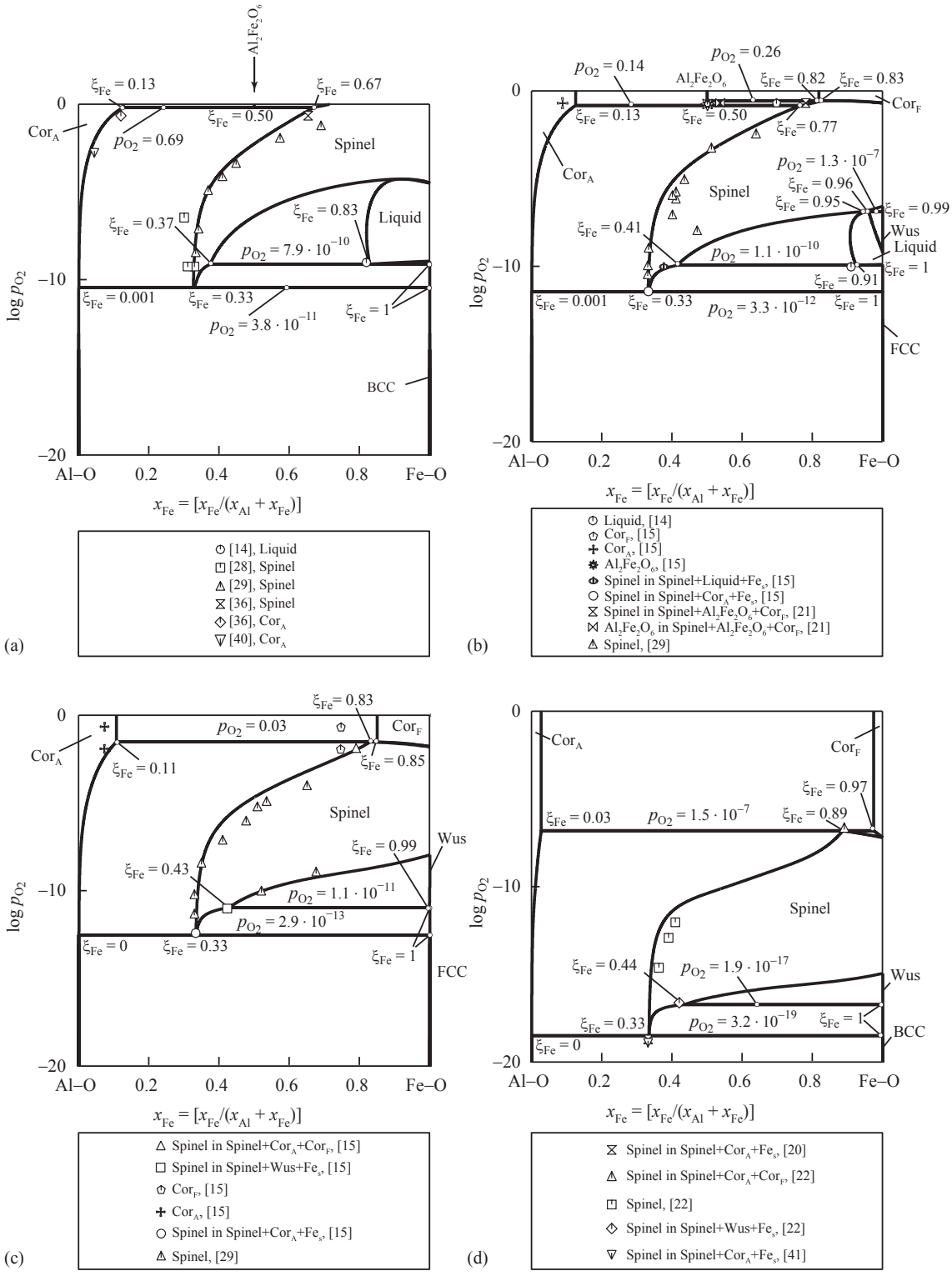

Fig. 9. Calculated potential diagrams for the Al_2O_3–Fe_2O_3–FeO system: (a) T = 1500 °C; (b) T = 1380 °C; (c) T = 1280 °C; (d) T = 900 °C. Continuous lines are the results of calculations according to this work; symbols correspond to experimental values. The designation "Fe_s" is given for solid iron.

4. Optimization procedure, results, and discussion

All calculations have been performed using the software package Thermo-Calc and the PARROT module for the optimization [66]. The set of the thermodynamic parameters obtained in this work is listed in Table 4.

The optimization was conducted in several stages. At first, the spinel phase was considered as simple stoichiometric hercynite.

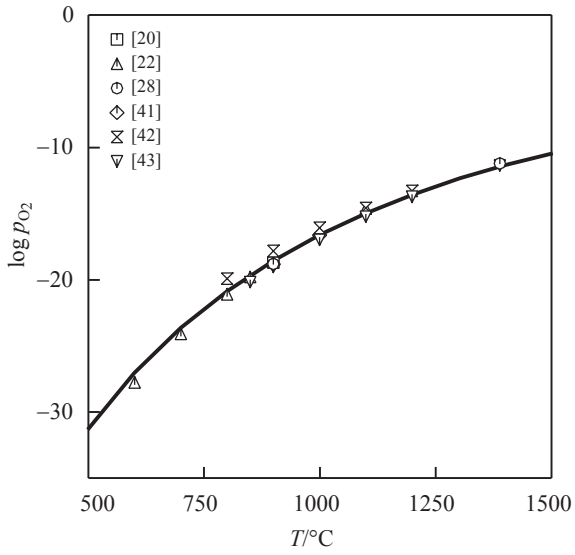

Fig. 10. Calculated oxygen potential for the three-phase equilibria $spin_h + cor_A$ + solid iron (continuous lines) and experimental values (symbols) at different temperatures.

Accordingly, the experimental values of liquidus and solidus temperatures for the Al_2O_3–FeO section in equilibrium with iron [14,27,37–39], data on the inversion degree of hercynite [23–26], and the results on the thermodynamic properties [43–48] in combination with data from Refs. [49–55] were employed for the evaluation. The parameters a_1, a_2 for spinel were assessed at this stage. For ionic liquid, ${}^0L_{Fe^{+2}:O^{-2},AlO_{1.5}}$, ${}^1L_{Fe^{+2}:O^{-2},AlO_{1.5}}$ parameters were also assessed at this stage to be able to reproduce phase equilibria with the liquid phase. For the estimation of the parameters, the data of [45,46] were additionally used. The agreement between experiment and calculations is satisfactorily only in case of [45] (Fig. 2). The future development of the model does not allow to improve the description of the data of [46]. The calculated heat capacity and enthalpy of formation from pure elements, the standard entropy of hercynite are given in Fig. 3 and Table 5, respectively. The calculated C_p values are in excellent agreement with data [47,48,55]. The calculated S°_{298} value is close to that of [48] while the good agreement with the data of [50–52,55] was obtained for the $\Delta_f H_{298}$ from pure elements. The correspondence between the calculated and experimental data on the cation distribution in hercynite [23–26] is good up to 900 °C (Fig. 4). At higher temperatures, the proposed model of spinel results in an overestimation of the results of [25,26]. Unlike to the thermodynamic assessments [8,9], our model predicted the congruent melting of hercynite with subsequent eutectic reaction for the Al_2O_3–FeO section in equilibrium with iron at this stage. This representation of the phase equilibria was not changed at further steps of the optimization procedure and supported by the data of [14,27,38,39] (Fig. 5). Taking into account accuracy of the used methods and scatter of the experimental data of [14,27,37–39], the eutectic or peritectic melting of hercynite can be regarded as equally possible. Since the key information that allows to make a final decision as to the type of melting of hercynite is absent in the literature, the additional investigation of this particular phase equilibrium is very desirable. It should be also mentioned that calculations in the system Al_2O_3–FeO reveal stabilization of single phase liquid at temperatures above 2560°C and concentration of Al_2O_3 of ~53 mol.%. Since there are no experimental data at these temperatures, all the calculations at temperatures higher than 2400°C must be considered as approximate.

At this stage, the ternary interaction parameters for corundum, hematite, and wüstite were preliminary assessed using the data on the solubility of FeO in corundum [14,27], liquidus and solidus temperatures [14,27,37] for the Al_2O_3–FeO section in equilibrium with iron. The agreement with the experimental data was satisfactory except for the data of [14] on the solubility of Al_2O_3 in wüstite.

At the second stage, the cations Fe^{+3} were introduced in the thermodynamic model of spinel to describe the stoichiometric magnetite and continuous solid solutions between hercynite and magnetite. The relevant parameters ΔG_2 and ΔG_3 for the spinel phase were assessed using the data for the three-phase equilibria involving spinel for the Al_2O_3–Fe_2O_3 section in air and pure oxygen [15,20,21], for the isothermal sections [15,20,22,28], for the Al_2O_3–FeO section in equilibrium with iron [14,27,37–39], for the partial pressures of oxygen [22,29–31,41–43], and for the cation distribution in spinel solid solution [32–34]. The interaction parameters ${}^0L_{Al^{+3},Fe^{+2}:Al^{+3}}$, ${}^0L_{Al^{+3}:Al^{+3},Fe^{+2}}$, ${}^0L_{Fe^{+2}:Al^{+3},Fe^{+2}}$, ${}^0L_{Al^{+3},Fe^{+2}:Fe^{+2}}$ were also introduced that allows compatibility of the ${}^\circ G_{Al^{+3}:Al^{+3}}$ parameter and parameters originating from the Fe–O thermodynamic description of [13]. It should be noted that when the Gibbs energy of end-members from different datasets are combined ΔG of several reciprocal reactions become fixed, and the introduction of mixing parameters are necessary to reproduce experimental data. The ${}^0L_{AlO_{1.5},FeO_{1.5}}$, ${}^1L_{AlO_{1.5},FeO_{1.5}}$, ${}^0L_{Fe^{+2}:O^{-2},AlO_{1.5},FeO_{1.5}}$, ${}^1L_{Fe^{+2}:O^{-2},AlO_{1.5},FeO_{1.5}}$, ${}^2L_{Fe^{+2}:O^{-2},AlO_{1.5},FeO_{1.5}}$ parameters have to be added for liquid phase to keep the proper description of the liquidus temperatures [14,21,27,37–39].

The coefficients from C to E of Equation (6) for $Al_2Fe_2O_6$ were fitted using the information on heat capacity [44] while coefficients A and B for this phase were fitted using the data on the enthalpy of formation and standard entropy [44] and phase equilibria from Refs. [15,18,19,21,36]. Some points related to the thermodynamic properties of this phase must be discussed. In the course of our calculations, we accepted coefficients of [44] for the heat capacity (Fig. 6). It was then evident that using heat capacity data from Ref. [44] it is impossible to get the satisfactory consistency of $\Delta_f H_{298}$ and S°_{298} with the phase equilibria including $Al_2Fe_2O_6$. Since the amount of the data for the phase relations is higher than for thermodynamic properties and S°_{298} function was not actually experimentally determined, we focused on the proper reproducing of phase relations (Fig. 7) by setting higher weight to them. Thus, the agreement between calculated and experimental values of $\Delta_f H_{298}$ from oxides, and estimated value of S°_{298} is not good (Table 5). The reason for such inconsistency can be in the extrapolation of the Gibbs energies derived at high temperature to room temperature using heat capacity [44]. Our calculations show that the description of S°_{298} can be improved (the calculated value 199.7 J mol^{-1} K^{-1}) while no significant improvement can be obtained in the description of $\Delta_f H_{298}$ (the calculated value 77400 J mol^{-1}) if the coefficients of $C_p(T)$ for $Al_2Fe_2O_6$ are fitted from the Neumann-Kopp equation with subtracted magnetic contribution. The respective calculated values of heat capacity are shown with dashed lines in Fig. 6. This implies internal disagreement between the experimental results for C_p and $\Delta_f H_{298}$ of $Al_2Fe_2O_6$ compound. It should be also noted, that experimental values for C_p are much higher than that predicted from the Neumann-Kopp equation (Fig. 6) that causes some doubts on the accuracy of the relevant measurements. It should be also mentioned that the thermodynamic data are available only for stoichiometric compound. Some additional investigations on the thermodynamic properties of the phase are strongly required. The parameters for wüstite, corundum, and $Al_2Fe_2O_6$ phase were finally adjusted using the data of [15,17–19,21,22].

The calculated cations distribution between tetrahedral and octahedral sites in spinel solid solution is shown in Fig. 8. Within

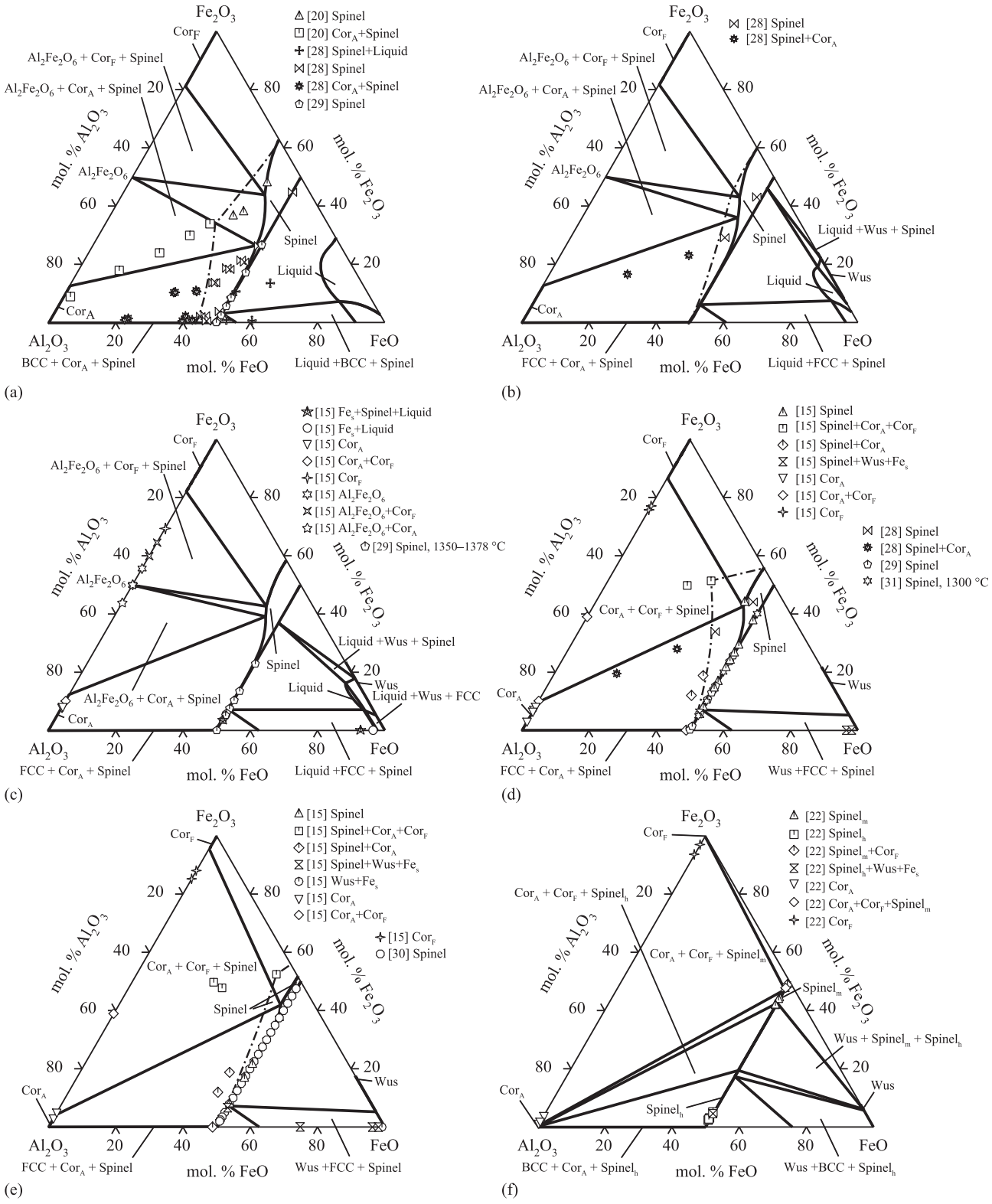

Fig. 11. Calculated isothermal sections of the Al_2O_3–Fe_2O_3–FeO system: (a) T = 1500 °C; (b) T = 1400 °C; (c) T = 1350 °C; (d) T = 1250 °C; (e) T = 1000 °C; and (f) T = 600 °C. Continuous lines are calculated phase boundaries according to this work; symbols correspond to experimental values. Dashed-dot line is an artificial line drawn to be compatible with the experimental data on the spinel homogeneity range at given temperature. The designation "Fe_s" is given for solid iron.

the proposed model of spinel phase, a good description was obtained for the data of [32] on the amount of Fe^{+3} cations on tetrahedral or octahedral sublattices at 1000 °C and for the results of [33,34] on the amount of Al^{+3} cations on tetrahedral or octahedral sublattices at 1325, 1327 °C. The experimental points on the distribution of Fe^{+2} cations [32,34] cannot be reproduced by the

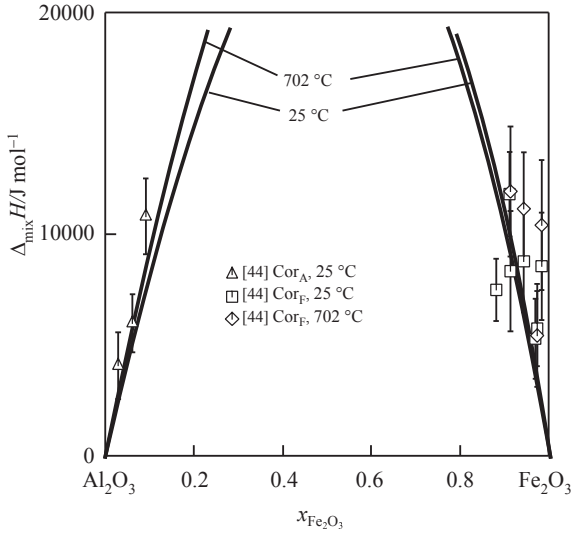

Fig. 12. Calculated mixing enthalpies in the hematite–corundum solid solution at 25 and 702 °C, $\Delta_{mix}H$, in comparison with experimental data. The standard reference states of Fe_2O_3 and Al_2O_3 are pure solid components.

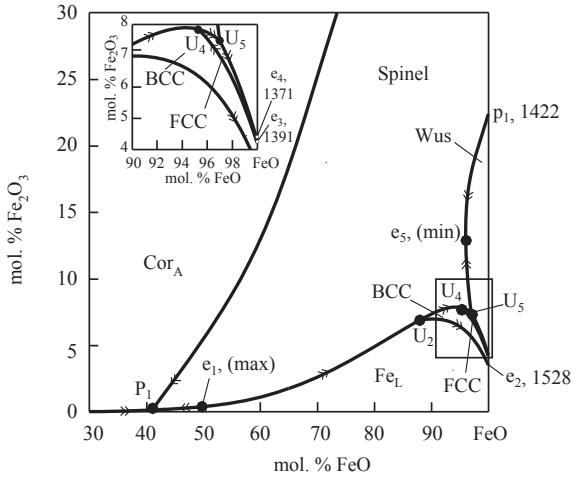

Fig. 13. Calculated partial liquidus projections of the Al_2O_3–Fe_2O_3–FeO system. The equilibria involving gas phase are excluded.

present calculations. In the whole, the qualitative agreement with the character of cations distribution between tetrahedral and octahedral sites in spinel solid solution was obtained in the present work.

The invariant reactions for the Al_2O_3–Fe_2O_3 sections at different partial pressures of oxygen and the Al_2O_3–FeO section in equilibrium with iron are shown in Figs. 5 and 7 and in Tables 6–8. For these sections, the description of the liquidus temperatures [14,21,27,37–39] is as good as in the thermodynamic assessment of [9]. However, the temperatures of invariant equilibria liquid + cor$_A$ + liquid iron + spinel and liquid + FCC + wüstite + spinel are higher by 20 °C than experimental one [14,27,37–39] (Fig. 5). On another hand, the calculated partial pressures of oxygen at which continuous solid solution of spinel can exist are in good agreement with data of [22,29] for the temperature range 900–1500 °C (Fig. 9). The p_{O_2} values [22,29,41–43] for the spin$_h$ + solid iron + cor$_A$ equilibrium were also successfully reproduced in the present work (Figs. 9 and 10). At medium p_{O_2} values, spinel compositions close to pure hercynite are

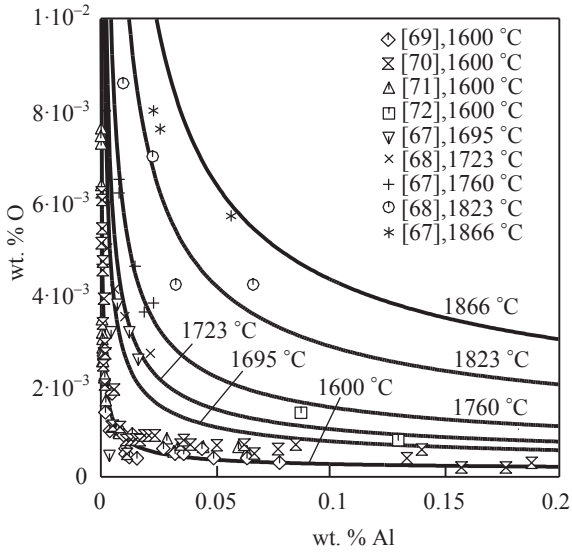

Fig. 14. Calculated solubility of aluminium and oxygen in liquid iron in equilibrium with corundum at different temperatures. Continuous lines are the results of calculations; symbols correspond to experimental values.

in equilibrium with liquid phase and solid or liquid iron at temperatures higher than invariant point liquid + FCC + wüstite + spinel and with wüstite and solid iron at temperatures below this invariant point (Fig. 9). The composition of spinel solid solution in equilibrium with wüstite and solid iron is changing towards higher concentration of Al_2O_3 with increasing temperature (Fig. 11d–f), and the equilibrium spinel composition is in good agreement with data of [15]. At high partial pressures of oxygen, spinel solid solution equilibrates with hematite and corundum (Fig. 9c,d), or with hematite and $Al_2Fe_2O_6$, and with corundum and $Al_2Fe_2O_6$ (Fig. 9a, b) depending on temperature.

In general, the reproducibility of the experimental data at low temperatures is not good. According to our calculations, spinel solid solution decomposes into hercynite-based and magnetite-based spinels at 672 °C and 18 mol.% Al_2O_3, 32 mol.% Fe_2O_3, 50 mol.% FeO. This temperature is very low in comparison with 860 °C [22]. The good description was obtained only for the three-phase equilibria spin$_m$ + cor$_A$ + cor$_F$ (Fig. 11f) and invariant point spin$_m$ + spin$_h$ + wüstite + BCC (point U_8 in Table 8). The calculated temperature of U_8 of 586 °C is in a satisfactory agreement with that given by Turnock and Eugster [22]. Combining their data with datapoints of [15], Turnock and Eugster [22] determined the coordinates for this ternary invariant point as 590 °C at 45.5 mol.% Al_2O_3, 4.5 mol.% Fe_2O_3, 50 mol.% FeO (for spin$_h$), 6.5 mol.% Al_2O_3, 43.5 mol.% Fe_2O_3, 50 mol.% FeO (for spin$_m$), and $p_{O_2} = 10^{-25}$ atm.

According to the present work, the solubility of Al_2O_3 in wüstite is low that is in good agreement with [15,16]. At temperature 1350 °C, wüstite is in equilibrium with liquid and FCC phase that is confirmed by the data of [15] (Fig. 10c). Our calculations show that the solubility of FeO in corundum is very low that is in satisfactory agreement with the observations of Novokhatsky et al. [27]. For the corundum and hematite, there is a good agreement between the calculated and experimental values of mixing enthalpies of solid solutions (Fig. 12). It is should be noted that this thermodynamic function is slightly increasing as the temperature is decreasing due to the magnetic contribution to the thermodynamic function of corundum. The data on the solubility of Fe_2O_3 in corundum [15,17–19,21,22] was also satisfactorily described in the present work (Fig. 7). As for the solubility of Al_2O_3 in hematite, the obtained

thermodynamic models of the phases result in the values close to that of [21]. For the solubility data of [15,17,19,22], the agreement between the experimental results and calculations is poor. It is hard to explain what causes such discrepancies keeping in mind that the description of the solubility of Fe_2O_3 in corundum is satisfactory (Fig. 7b). Comparing the data on the mixing enthalpy in hematite-corundum solid solution (Fig. 12) with the experimental data on the mutual solubility of corundum and hematite it can be noted that $\Delta_{mix}H$ function is almost symmetrical with respect to equiatomic composition. This implies that the solubility of Fe_2O_3 in corundum could not be larger than the solubility of Al_2O_3 in hematite.

For $Al_2Fe_2O_6$ compound, the calculated high-temperature limit of the phase stability at $p_{O_2} = 0.21$ atm. falls fairly good to the experimental value of [21] (Fig. 7, Table 7). At $p_{O_2} = 1$ atm., the calculated high-temperature limit of stability of $Al_2Fe_2O_6$ compound is by 35 °C higher than the experimentally observed. The temperature of the invariant point spinel + $Al_2Fe_2O_6$ + cor_F established in Ref. [21] is not very well reproduced in the calculation. However, the calculated phase compositions are close to the experimental values (Tables 6 and 7) especially for the Al_2O_3–Fe_2O_3 section in air. According to the calculations in the present work, the low-temperature stability limit of $Al_2Fe_2O_6$ is 1317 °C both at $p_{O_2} = 0.21$ and 1 atm. that is in good agreement with [15,21]. As to this temperature, Muan and Gee [21] and Atlas and Sumida [15] encountered the problem of precise determination of the exact value. Muan and Gee [21] could not synthesize the phase even under hydrothermal conditions until a temperature of 1318 °C was reached but once formed (at temperatures higher than 1318 °C) it did not decompose to pure oxides at lower temperatures. The authors attributed this to the extreme sluggishness of the reactions at low temperatures and supposed that the phase should be stable below 1318 °C. Atlas and Sumida [15] could not obtain $Al_2Fe_2O_6$ phase below 1320 °C in air from the mixed or co-precipitated oxides. Taking into account slow kinetics of solid state reactions and complexity of the equilibrium relations due to the formation of intermediate structure, Atlas and Sumida [15] proposed 1320 °C as a low-temperature stability limit of $Al_2Fe_2O_6$. Muan [36] used an indirect method to establish a low-temperature stability limit of $Al_2Fe_2O_6$. Combining their own data with datapoints obtained in Ref. [21], the authors determined this limit as an intersection point of two lines $\log p_{O_2}$ versus $1/T$ corresponding to the reactions hematite + $Al_2Fe_2O_6$ = 2spinel + $1/2O_2$ and $2Al_2Fe_2O_6$ = corundum + 2spinel + $1/2O_2$. The obtained coordinates are 1315 °C at $p_{O_2} = 0.03$ atm. Muan [36] concluded that the lower temperature stability limit of $Al_2Fe_2O_6$ ($Al_2Fe_2O_6 = Al_2O_3 + Fe_2O_3$) is 1318 °C in air and at 1 atm. O_2 because all the oxides are in the highest valence state at these conditions. There was no discussion of any difficulties concerning the phase synthesis from pure oxides in work of Rhamdhani et al. [19] who show that this phase is stable at a temperature of 1300 °C. So, the question as to the low-temperature stability limit of $Al_2Fe_2O_6$ requires more experimental consideration.

At the third stage, the vacancy was added in the second sublattices of the spinel phase to model deviation from Fe_3O_4–$FeAl_2O_4$ stoichiometry in the direction Al_2O_3 and Fe_2O_3. Then, all the derived parameters of the liquid and spinel phases were temporarily fixed, and the ${}^0L_{Al^{+3}:Fe^{+2},Va}$, ${}^0L_{Al^{+3}:Fe^{+3},Va}$ parameters were optimized by adding the experimental data relative to the excess solubility of oxygen in spinel [14,15,20,21,27,29]. At last, the interaction thermodynamic parameters of liquid, wüstite, corundum, and $Al_2Fe_2O_6$ phases were finally adjusted to obtain the best fit to the experimental equilibria.

From Fig. 11, it is evident that very high excess solubility of oxygen (deviation from Fe_3O_4–$FeAl_2O_4$ stoichiometry in the direction Al_2O_3 and Fe_2O_3) in spinel continuous solid solution (shown with hypothetical dashed-dot line) [15,20,28] cannot be described within the present thermodynamic assessment. It should be noted that the dataset of [20] was obtained from the direct weighing method, and the dataset of [28] was the result of thermogravimetric measurements that do not imply high accuracy of the experimental data. Most of the results show that predominantly magnetite-based spinel solid solutions dissolve great amount of excess oxygen (Fig. 11a–e). According to our calculations, the maximum extension of spinel solid solution corresponds to the three-phase equilibrium at given temperature that agrees with the results of [15]. This extension is decreasing with temperature. The excess solubility of Al_2O_3 in hercynite calculated according to the present work is in good agreement with data of [14,27].

The calculated liquidus projection is shown in Fig. 13. Additionally to the experimentally established invariant points P_1, e_1 and U_5, the model predicts eutectic minimum, e_5, at 1338 °C in the monovariant line liquid + wüstite + spinel of the liquidus surface. The model also predicts five invariant reactions related to the transformation in metallic iron. Three of these reactions are associated with the polymorphic transformation of iron from BCC to FCC (namely, U_4, U_6 and U_7 in Table 8). The invariant reactions U_1 and U_2 at 1538 °C and 1532 °C related to the transformation of iron from liquid to solid state (Fig. 4, Table 8).

The thermodynamic database obtained in this work includes liquid phase described by the partially ionic liquid model, which allows the description of both metallic and oxide liquid as a single phase. This description based on the binary parameters [13,60,63–65,73] and ternary parameter [7] was used to calculate the solubility of aluminium and oxygen in metallic liquid in equilibrium with corundum and compared with experimental data [67–72]. The obtained results presented in Fig. 14 are very similar to calculations of [7] and reproduce experimental data well. However, more experimental data for the interaction between metallic and ceramic parts must be considered and compared with the calculations.

5. Conclusions

The thermodynamic description of the Al_2O_3–Fe_2O_3–FeO system has been developed, and different kinds of phase diagrams are calculated. The spinel phase was described using the four-sublattice formula. The proposed model allows to describe stoichiometric magnetite (inverse spinel at room temperature) and hercynite (normal spinel at room temperature), their tendency towards disordering with temperature increasing, and solubility of Fe_2O_3 and Al_2O_3 components in spinel solid solution. Calculated values of the thermodynamic functions, vertical and isothermal sections, potential diagrams are compared to experimental data from various sources. A good agreement has been achieved between our thermodynamic description and experimental data. The whole set of the new optimized thermodynamic parameters for oxide part of the system is presented. Thermodynamic database obtained in the present work allow the calculation of the interface reactions between steel and alumina at different oxygen partial pressures accounting possibility of different oxide phase formation which is very important for the processes of steel filtration, foundry production, and metallurgy. A future step in our work is a combination of current database with the thermodynamic assessments of metallic phases in the Al–Fe and Al–O systems to get a description of the whole Al–Fe–O system and to calculate phase equilibria including the metallic side of the system in very wide range of oxygen partial pressures. It should be emphasized that the intended introduction of the descriptions for the solution fcc, bcc phases and intermetallics does not significantly influence the results obtained

in the present work due to the stability of almost pure iron and Al_2O_3 in a wide range of oxygen partial pressures.

Acknowledgment

The authors would like to thank the German Research Foundation (DFG) for financial support of the investigations in the project A03 of the Collaborative Research Centre SFB 920. L. Dreval is grateful to DFG for supporting of her stay in TU Bergakademie Freiberg for performing this work.

References

[1] D. Janke, Z.T. Ma, P. Valentin, A. Heinen, Improvement of castability and anality of continuously cast steel, ISIJ Int. 40 (2000) 31–39.
[2] K. Sasai, Y. Mizukami, Mechanism of alumina adhesion to continuous caster nozzle with reoxidation of molten steel, ISIJ Int. 41 (2001) 1331–1339.
[3] J. Mei, R.D. Halldearn, P. Xiao, Mechanisms of the aluminium-iron oxide thermite reaction, Scr. Mater 41 (1999) 541–548.
[4] K. Nakashima, K. Takihira, K. Mori, N. Shinozaki, Wettability of Al_2O_3 substrate by liquid iron – effects of oxygen in liquid iron and purity of Al_2O_3 substrate, J. Jpn. Inst. Met. 55 (1991) 1199–1206 (in Japanese).
[5] E. Kapilashrami, A. Jakobsson, A.K. Lahir, S. Seetharaman, Studies of the wetting characteristics of liquid iron on dense alumina by X-ray sessile drop technique, Metall. Mater. Trans. B 34B (2003) 193–199.
[6] F.H. Stott, K.T. Chuah, L.B. Bradley, in: H.J. Grabke, M. Schütze (Eds.), Oxidation-Sulfidation of Iron Aluminides, Oxidation of Intermetallics, first ed., Wiley-VCH, 1998, pp. 221–231.
[7] T. Zienert, S. Dudczig, O. Fabrichnaya, C.G. Aneziris, Interface reactions between liquid iron and alumina-carbon refractory filter materials, Ceram. Int. 41 (2) (2015) 2089–2098.
[8] G. Eriksson, P. Wu, A. Pelton, Critical Evaluation and Optimization of the Thermodynamic properties and phase diagrams of the MgO–Al_2O_3, MnO–Al_2O_3, FeO–Al_2O_3, Na_2O–Al_2O_3 and K_2O–Al_2O_3 systems, CALPHAD: Comput. Coupling Phase Diagrams Thermochem. 17 (2) (1993) 189–205.
[9] S.A. Decterov, I.-H. Jung, E. Jak, Y.-B. Kang, P. Hayes, A.D. Pelton, Thermodynamic modeling of the Al_2O_3–CaO–CoO–CrO–Cr_2O_3–FeO–Fe_2O_3–MgO–MnO–NiO–SiO_2–S system and applications in ferrous process metallurgy, in: VII International conference on molten slags fluxes and salts, January 25–28, 2004 (Johannesburg), S. Afr. Inst. Min. Metall., 2004, pp. 839–850.
[10] F.A. Elrefaie, W.W. Smeltzer, Thermodynamics of the system Iron-Aluminium-Oxygen between 1073 K and 1573 K, Metall. Trans. B 14B (1983) 85–93.
[11] O. Kubaschewski, R. Schmid-Fetzer, L. Rokhlin, L. Cornish, O. Fabrichnaya, in: G. Effenberg, S. Ilyenko (Eds.), Aluminium–Iron–Oxygen, Landolt-Börnstein – Group IV Physical Numerical Data and Functional Relationships in Science and Technology Chemistry, Springer-Verlag Berlin Heidelberg, 2008, pp. 1–40.
[12] K.P. Trumble, Thermodynamic analysis of aluminate formation at Fe/Al_2O_3 and Cu/Al_2O_3 interfaces, Acta Metall. Mater. 40 (Suppl.) (1992) S105–S110.
[13] B. Sundman, An assessment of the Fe–O system, J. Phase Equilib. 12 (1) (1991) 127–140.
[14] W.A. Fischer, A. Hoffman, Das Zustandsschaubild Eisenoxydel–Aluminiumoxyd (The phase diagram ferrous oxide–aluminium oxide), Arch. Eisenhuettenwes 27 (1956) 343–346 (in German).
[15] L.M. Atlas, W.K. Sumida, Solidus, subsolidus and subdissociation phase equilibria in the system Fe-Al-O, J. Am. Ceram. Soc. 41 (5) (1958) 150–160.
[16] G. Schmahl, H. Dillenburg, Gleichgewichtsuntesuchungen an eisenoxidhaltigen Mischphasen innerhalb der Dreistoffsysteme Fe–Al–O, Fe–Cr–O und Fe–V–O (Equilibrium studies of iron oxide containing solid solutions in the ternary systems Fe–Al–O, Fe–Cr–O and Fe–V–O), Z. Phys. Chem. 65 (1969) 119–138 (in German).
[17] A.K. Ladavos, T.V. Bakas, The Al_2O_3–Fe_2O_3 mixed oxidic system, I. Preparation and characterization, React. Kinet. Catal. Lett. 73 (2) (2001) 223–228.
[18] R. Hansson, P.C. Hayes, E. Jak, Experimental study of phase equilibria in the Al–Fe–Zn–O system in air, Metall. Mater. Trans. B 35B (2004) 633–642.
[19] M.A. Rhamdhani, T. Hidayat, P.C. Hayes, E. Jak, Subsolidus phase equilibria of Fe–Ni–X–O (X = Mg, Al) systems in air, Metall. Mater. Trans. B 40B (2009) 25–38.
[20] R.G. Richards, J. White, 13. Phase relationships of iron-oxide-containing spinels. Part I. Relationships in the system Fe–Al–O, Trans. Br. Ceram. Soc. 53 (1954) 233–270.
[21] A. Muan, C.L. Gee, Phase equilibrium studies in the system iron oxide–Al_2O_3 in air and at one atmosphere oxygen pressure, J. Am. Ceram. Soc. 39 (1956) 207–214.
[22] A.C. Turnock, H.P. Eugster, Fe-Al Oxides: phase relationships below 1000 °C, J. Pet. 3 (3) (1962) 533–565.
[23] R.J. Hill, X-ray powder diffraction profile refinement of synthetic hercynite, Am. Mineral. 69 (1984) 937–942.
[24] S.R. Bohlen, W.A. Dollase, V.J. Wall, Calibration and applications of spinel equilibria in the system FeO–Al_2O_3–SiO_2, J. Pet. 27 (1986) 1143–1156.
[25] R.J. Harrison, S.A.T. Redfern, H.St.C. O'Neill, The temperature dependence of the cation distribution in synthetic hercynite ($FeAl_2O_4$) from in-situ neutron structure refinements, Am. Mineral. 83 (1998) 1092–1099.
[26] L. Larsson, H. St C. O'Neil, H. Annersten, Crystal chemistry of synthetic hercynite ($FeAl_2O_4$) from XRD structural refinements and Mössbauer spectroscopy, Eur. J. Mineral. 6 (1994) 39–51.
[27] I.A. Novokhatsky, B.F. Belov, Phase equilibria and distribution of elements in the Fe–O–Al system, Izv. Akad. Nauk. SSSR, Met. 1 (1966) 38–48.
[28] B.D. Roiter, Phase equilibria in the spinel region of the system FeO–Fe_2O_3–Al_2O_3, J. Am. Ceram. Soc. 47 (10) (1964) 509–511.
[29] C.E. Meyers, T.O. Mason, W.T. Petuskey, J.W. Halloran, H.K. Bowen, Phase equilibria in the system Fe–Al–O, J. Am. Ceram. Soc. 63 (11–12) (1980) 659–663.
[30] A.A. Lykasov, A.A. Kimyashev, Activities of the components in a spinel solid solution of the Fe–Al–O system, Russ. J. Phys. Chem. A 85 (9) (2011) 1495–1498.
[31] A. Petric, K.T. Jacob, C.B. Alcock, Thermodynamic properties of Fe_3O_4–$FeAl_2O_4$ spinel solid solutions, J. Am. Ceram. Soc. 64 (11) (1981) 632–639.
[32] J. Nell, B.J. Wood, T.O. Mason, High-temperature cation distributions in Fe_3O_4–$MgAl_2O_4$–$MgFe_2O_4$–$FeAl_2O_4$, Am. Mineral. 74 (1989) 339–351.
[33] G. Dehe, B. Seidel, K. Melzer, C. Michalk, Determination of a cation distribution model of the spinel system $Fe_{3-x}Al_xO_4$, Phys. Status Solidi A 31 (1975) 439–447.
[34] T.O. Mason, High-temperature cation distributions in Fe_3O_4–$FeAl_2O_4$, J. Am. Ceram. Soc. 68 (3) (1985) C74–C75.
[35] M. Schieber, R.B. Frankel, N.A. Blum, S. Foner, High-magnetic-field studies of orthorhombic and rhombohedral $Al_{2-x}Fe_xO_3$ compounds, J. Appl. Phys. Melv. N. Y. U.S. 38 (1967) 1282–1283.
[36] A. Muan, On the stability of the phase Fe_2O_3.Al_2O_3, Am. J. Sci. 256 (1958) 413–422.
[37] W. Oelsen, G. Heynert, Die Reaktionen zwischen Eisen–Mangan–Schmelzen und den Schmelzen ihrer Aluminate (The reaction between iron-manganese melts and melting of their aluminate), Arch. Eisenhuettenwes 26 (10) (1955) 567–575 (in German).
[38] F.Ya Galakhov, Alumina regions of ternary aluminosilicate systems. Communication 1. The Systems FeO–Al_2O_3–SiO_2 and MnO–Al_2O_3–SiO_2, Izv. Akad. Nauk. SSSR, Otd. Khim. Nauk. 5 (1957) 525–531 (in Russian).
[39] K. Rosenbach, J.A. Schmitz, Untersuchungen in Dreistoffsystem Eisen(II)-oxid–Chrom(III)-oxid–Tonerde (Investigations in the ternary system iron(II)-oxide–chromium(III)-oxide–alumina), Arch. Eisenhuettenwes 45 (1974) 843–847 (in German).
[40] T.M. Pollak, High Temperature Electrical Conductivity and Defect Chemistry of Iron-doped Alumina, Ph.D. thesis, Massachusets Inst. Technology, 1976.
[41] V. Cirilli, Studio dell' equilibrio di riduzione con ossido di carbonio, degli ossidi di ferro on presenza di alumina (The investigation of the equilibrium reduction of the iron oxide with carbon monoxide in the presence of alumina), Gazz. Chim. Ital. 76 (1946) 339–344 (in Italian).
[42] A. McLean, R.G. Ward, Thermodynamics of hercynite formation, J. Iron Steel Inst. 204 (1966) 8–11.
[43] J.C. Chan, C.B. Alcock, K.T. Jacob, Electrochemical measurements of the oxygen potential of the system iron–alumina–hercynite in the temperature range 750 to 1600 °C, Can. Metall. Q. 12 (1973) 439–443.
[44] J. Majzlan, A. Navrotsky, B.J. Evans, Thermodynamics and crystal chemistry of the hematite–corundum solid solution and the $FeAlO_3$ phase, Phys. Chem. Miner. 29 (2002) 515–526.
[45] S. Ban-Ya, A. Chiba, A. Hikosaka, Thermodynamics of Fe_tO–M_xO_y (M_xO_y = CaO, SiO_2, TiO_2 and Al_2O_3) binary melts saturated with solid iron, in: Australia Japan Extractive Metallurgy Symposium, July 16–18, 1980 (Sydney), Australian Inst. Min. Metall.. 23, 1980, pp. 457–467.
[46] P. Fredriksson, S. Seetharaman, Thermodynamic activities of "FeO" in some binary "FeO"-containing slags, Steel Res. Int. 75 (4) (2004) 240–246.
[47] E.G. King, Heat capacities at low temperatures and entropies of five spinel minerals, J. Phys. Chem. 60 (1956) 410–412.
[48] S. Klemme, J.C. Van Miltenburg, Thermodynamic properties of hercynite ($FeAl_2O_4$) based on adiabatic calorimetry at low temperatures, Am. Mineral. 88 (2003) 68–72.
[49] R.A. Robie, B.S. Hemingway, J.R. Fisher, Thermodynamic properties of minerals and related substances at 298.15 K and 1 bar (10^5 pascals) pressure and at higher temperatures, in: U. S. Geol. Surv. Bull. 1452, U. S. Government Printing Office, Washington, 1979.
[50] T.J.B. Holland, R. Powell, An enlarged and updated internally consistent thermodynamic dataset with uncertainties and correlations – the system K_2O–Na_2O–CaO–MgO–MnO–FeO–Fe_2O_3–Al_2O_3–TiO_2-SiO_2-C-H_2-O_2, J. Metamorph. Geol. 8 (1990) 89–124.
[51] R.O. Sack, M.S. Ghiorso, An internally consistent model for the thermodynamic properties of Fe–Mg–Titanomagnetite–Aluminate spinels, Contrib. Mineral. Pet. 106 (1991) 474–505.
[52] M. Gottschalk, Internally consistent thermodynamic data for rock-forming minerals in the system SiO_2–TiO_2–Al_2O_3–Fe_2O_3–CaO–MgO–FeO–K_2O–Na_2O–H_2O–CO_2, Eur. J. Mineral. 9 (1997) 175–223.
[53] R.G. Berman, L.Y. Aranovich, Optimized standard state and solution properties of minerals.1. Model calibration for olivine, orthopyroxene, cordierite, garnet, ilmenite in the system FeO–MgO–CaO–Al_2O_3–TiO_2–SiO_2, Contrib. Mineral. Pet. 126 (1996) 1–24.
[54] T.J.B. Holland, R. Powell, An internally consistent thermodynamic data set for

phases of petrological interest, J. Metamorph. Geol. 16 (1998) 309–343.
[55] O. Fabrichnaya, S.K. Saxena, P. Richet, E.F. Westrum, Thermodynamic Data, Model and Phase Diagrams in Multicomponent Oxide Systems, Springer Verlag, Berlin Heidelberg, 2004, pp. 122–123.
[56] B. Hallstedt, Thermodynamic assessment of the system MgO–Al_2O_3, J. Am. Ceram. Soc. 75 (1992) 1497–1507.
[57] G. Inden, Determination of chemical and magnetic interchange energies in bcc alloys. III. Application to ferromagnetic alloys, Z. Met. 68 (1977) 529–534.
[58] M. Hillert, M. Jarl, A model for alloying effects in ferromagnetic metals, CALPHAD: Comput. Coupling Phase Diagrams Thermochem. 2 (3) (1978) 227–238.
[59] S.A. Degterov, E. Jak, P.C. Hayes, A.D. Pelton, Experimental study of phase equilibria and thermodynamic optimization of the Fe–Zn–O system, Metall. Mater. Trans. B 32B (2001) 643–657.
[60] T. Zienert, O. Fabrichnaya, Thermodynamic assessment and experiments in the system MgO–Al_2O_3, CALPHAD: Comput. Coupling Phase Diagrams Thermochem. 40 (2013) 1–9.
[61] M. Hillert, B. Jansson, B. Sundman, J. Ågren, A two-sublattice model for molten solutions with different tendency for ionization, Metall. Trans. A 16A (2) (1985) 261–266.
[62] B. Sundman, Modification of the two-sublattice model for liquids, CALPHAD: Comput. Coupling Phase Diagrams Thermochem. 15 (1991) 109–119.
[63] M. Selleby, B. Sundman, A re-assessment of the Ca–Fe–O system, CALPHAD: Comput. Coupling Phase Diagrams Thermochem. 20 (1996) 381–392.
[64] B. Hallstedt, Thermodynamic calculation of some subsystems of the Al–Ca–Mg–Si–O system, J. Phase Equilib. 14 (1993) 662–667.
[65] B. Sundman, I. Ohnuma, N. Dupin, U.R. Kattner, S.G. Fries, An assessment of the entire Al–Fe system including $D0_3$ ordering, Acta Mater 57 (2009) 2896–2908.
[66] B. Sundman, B. Jansson, J.O. Andersson, The Thermo-Calc databank system, CALPHAD: Comput. Coupling Phase Diagrams Thermochem. 9 (2) (1985) 153–190.
[67] N.A. Gokcen, J. Chipman, Aluminium–oxygen equilibrium in liquid iron, Trans. AIME 197 (1953) 173–178.
[68] A. McLean, H. Bell, Experimental study of the reaction$Al_2O_3+3H_2=3H_2O+2Al$, J. Iron Steel Inst. 203 (1965) 123–130.
[69] L.E. Rohde, A. Choudhury, M. Wahlster, New investigation of the aluminium–oxygen equilibrium in iron melt, Arch. Eisenhuettenwes 42 (1971) 165–174.
[70] D. Janke, W.A. Fischer, Deoxidation equilibria of Ti, Al and Zr in iron melts at 1600°C, Arch. Eisenhuettenwes 47 (1976) 195–198.
[71] S. Dimitrov, A. Weyl, D. Janke, Control of aluminium-oxygen reaction in pure iron melts, Steel Res. 66 (1995) 3–7.
[72] J.-D. Seo, S.-H. Kim, K.-R. Lee, Thermodynamic assessment of Al deoxidation reaction in liquid iron, Steel Res. 69 (1998) 49–53.
[73] A.T. Dinsdale, SGTE data for pure elements, CALPHAD: Comput. Coupling Phase Diagrams Thermochem. 15 (4) (1991) 317–425.